*REVISED Manuscript UNMARKED
Click here to view linked References

Part 1: Experimental Validation of a RANS-CFD Methodology for the Hydrodynamics of Wind-Assisted Ships Operating at Leeway Angles

N.J. van der Kolk[1], J.A. Keuning and R.H.M. Huijsmans

Ship Hydromechanics, Delft University of Technology, Mekelweg 2, 2628 CD, Delft, The Netherlands

Abstract: A Reynolds-averaged Navier Stokes computational fluid dynamics (RANS-CFD) package will be one of the primary tools used during the development of a performance prediction program for wind-assisted commercial ships. This paper is Part 1 of a two-part series describing the RANS-CFD method adopted for this study. The modelling challenge presented by large separated flow structures in the wake of a sailing ship points to a conscientious validation study. A validation data set, consisting of hydrodynamic forces acting on the ships sailing with a leeway angle, was collected at the Delft University of Technology towing tank facility, for bare-hull and appended cases. Appended cases were designed to represent a broad range of appendage typologies: Rudder, Bilge-keels, Skeg, and Barkeel. A validation statement is made for simulations for the entire bare-hull series and for appended geometries, excepting the Bilge-keel case. The simulation method is described in Part 2, including the assessment of the numerical uncertainty.

Keywords: Green shipping, Computational fluid dynamics, Validation, Sailing vessels, Ships, Climate change

1 INTRODUCTION

Wind as a source of energy for commercial ships has again garnered interest as an environmentally friendly propulsion alternative, as a possible response to volatile fuel prices, and to comply with increasingly exacting environmental regulations. The further development of this promising technology is hampered by a poor understanding of the interaction effects between wind propulsors and the hydromechanics of commercial ships. The Wind-Assisted Ship Propulsion (WASP) Performance Prediction Program, under development at Delft University of Technology, will provide designers and researchers the ability to explore the possibilities offered by wind as an auxiliary propulsor. The performance prediction tool is developed and documented in a rigorous and transparent way, so that the designer or researcher can confidently report performance figures for subsequent environmental and economic analyses.

The introduction of wind propulsors aboard commercial vessels will introduce forces and moments besides the desired forward thrust. For sailing equilibrium, the transvers component of the aerodynamic force must be opposed by a righting moment and a hydrodynamic sideforce. The

[1] Corresponding author. E-mail: n.j.vanderkolk@tudelft.nl, Tel.: +31 (0)152788729

© 2019. This manuscript version is made available under the CC-BY-NC-ND 4.0 license https://creativecommons.org/licenses/by-nc-nd/4.0/. Published version: https://doi.org/10.1016/j.oceaneng.2018.12.041

production of these reactionary forces gives rise to a steady heel angle and leeway angle. Vessel performance with leeway angles is characterised by an increase in resistance and by the generation of a strong, destabilising moment about the yaw axis, both of which are key design concerns. With the WASP Performance Prediction Program, a designer is able to perform parametric investigations for the arrangement of wind propulsors and the hull form geometry, and can eventually optimize a commercial hull form for sailing. For example, the well-known phenomenon of induced drag for lifting surfaces has a direct analogue for commercial ship types while generating hydrodynamic sideforce. Though the flow mechanisms only vaguely resemble the Prandtl wing and the associated derivation for the induced drag, the accounting for energy loss in shed vorticity is especially relevant for the present application. Following theories for low-aspect planforms (Jones, 1946), the induced drag may be significant for commercial ships, meaning that the thrust delivered by a wind propulsor might well be overwhelmed by this increase in resistance, negating the benefit of adding the wind propulsor. Models that capture the behaviour of a generic commercial vessel under sail will be derived by studying the sensitivity of vessel performance to changes in hull geometry. For example, to determine the influence of vessel draft, vessel behaviour for increased and decreased draft is fit to some functional form. Of course, as other hull-form parameters are allowed to vary, the structure of this function will become increasingly complex. The force models for a generic hull would be determined by polynomial regression techniques from a large set of systematically varied hulls. In the past, this database for regression analysis was built using results from towing tank experiments. (Keuning & Sonnenberg, 1998) The maturity of Reynolds-averaged Navier Stokes computational fluid dynamics (RANS-CFD) solvers offers the ready, inexpensive analysis for a large number of hull variations. However, simulations that remain computationally affordable may be unable to model the flow patterns occurring near a sailing commercial ship. Fluid flow around the wind-assisted ship operating at a leeway angle will experience separation effects and will become entrained in large vortices in the wake of the ship. Modelling the occurrence of separation and the evolution of these vortices is the principal simulation challenge, as both phenomena may challenge modelling assumptions made in the simulation setup.

In this paper, a validation exercise is described for the computationally affordable assessment of large numbers of ship-hull variations. This simulation work is performed in the service of a regression-based modelling for the performance of wind-assist vessels. Production runs are performed with a 6 million cell grid, which gave numerical uncertainties that were commensurate with the uncertainties in the experimental data. The results for this validation exercise are presented for bare-hull and appended-hull RANS-CFD simulations.

1.1 SIMULATION METHOD

The simulation method for the production runs is designed for the assessment of hull geometry variants of the Delft Wind-Assist Series. The level of grid refinement is such that the volume of simulations is feasible using the Cartesius supercomputer facility (Surf SARA, n.d.). The simulations methodology for the validation exercise is described briefly to provide context for the reader.

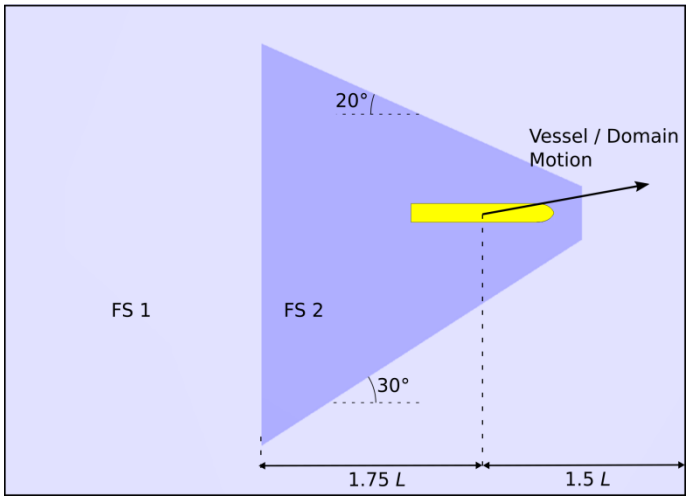


Figure 1 Computational domain for simulation. Note the skewed wedge for the wake refinement zone.

The Drift Sweep procedure (Toxopeus, 2011) was adopted for the efficient analysis of a series of leeway angles and speeds. The domain is meshed once, with the ship aligned with the x-axis, and assigned a prescribed motion (including a leeway angle) within a quiescent fluid, as in Figure 1. Simulation cases proceed from a converged solution to the next combination of leeway angle and vessel speed using a gradual transition, such that the time required for the convergence of the new solution is reduced compared with reinitializing the computation. Integrated fluid forces on the ship hull are determined in the coordinate system aligned with the direction of forward motion. Vessel response may be unsteady due to shedding behaviour around the hull, but only averaged forces are of interest within the context of this study. After the simulation has converged, an average is made over one characteristic time interval, equal to L/U.

The simulations are performed with the FINE/Marine suite, a commercial RANS-CFD package distributed by Numeca. The unsteady RANS equations are solved with the ISIS-CFD flow solver, developed at Ecole Centrale Nantes. The ISIS-CFD flow solver is an incompressible unsteady RANS method. The unstructured spatial discretization for the transport equations is based on the finite volume method. Free-surface flows are simulated with a conservation equation for the mass fraction. A detailed description of the solver is provided in (Deng, et al., 2005) (Deng, et al., 2006) (Duvigneau & Visonneau, 2003) (Queutey & Visonneau, 2007). Turbulence is modelled using the Explicit Algebraic Stress Model (EASM) to provide an anisotropic modelling that remains computationally affordable.

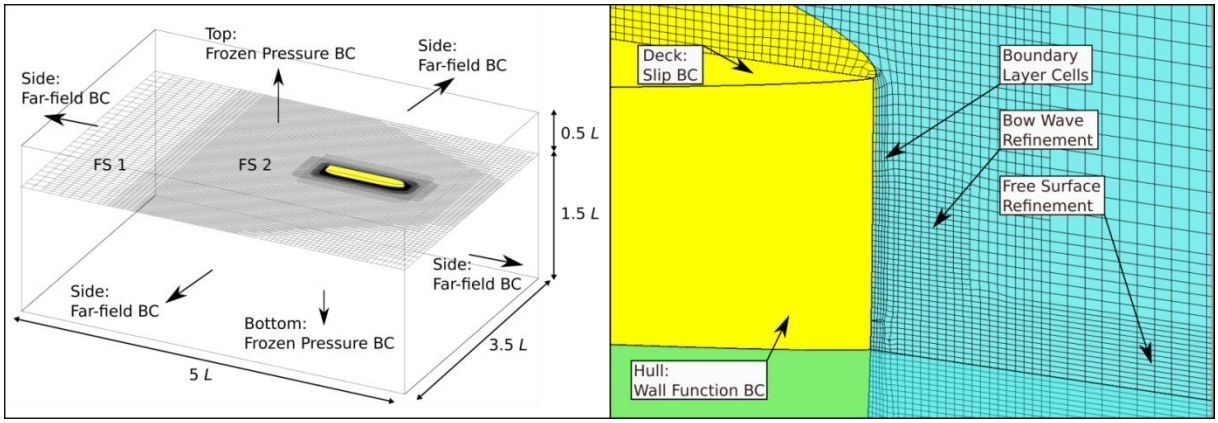


Figure 2 Boundary conditions and mesh details.

Simulation boundary conditions and meshing details are indicated in Figure 2. The boundary layer at the ship hull is modelled with a logarithmic wall function boundary condition. For model scale validation simulations, five boundary layer cells were sufficient to satisfy the modelling criterion for Y^+ value at the hull. As a single mesh is used for several operating conditions, the average Y^+ was between 30 and 60, depending on the Froude number, while the maximum Y^+ varies between 65 and 90 (located at the region of flow acceleration around the forward bilge). The mesh refinement level at the hull corresponds to 500 cells per ship length. The free-surface is refined to a level nine in the z-direction. A detailed description of the simulation method, meshing strategy, and the simulation verification exercise is presented in Part 2 of this publication.

2 VALIDATION DATA SET

The validation dataset is composed of hulls from the Delft Wind-Assist Series. Each hull and appended case is tested at three speeds: Froude number Fn= 0.128, 0.168, 0.21, corresponding to 9, 12, and 15 knots at full scale. At model scale, the vessel speed is equal to 0.65, 0.87, and 1.09 m/s. The full scale Reynolds number is approximately 8E8. The model scale Reynolds number is approximately 2.3E6. Four leeway angles: β= 0°, 3°, 6°, 9° were tested, giving a total of 12 operating conditions. The validation data consists of global forces acting on the ship: resistance X, sideforce Y, and yaw moment N. These are evaluated in a flow-aligned coordinate system.

2.1 DELFT WIND-ASSIST SERIES

The hulls in the wind-assist series are systematic variations of a wind-assist concept designed by Dykstra Naval Architects, of the Netherlands. The series comprises 42 hulls, for which the prismatic coefficient, the midship coefficient, the draft-to-length ratio, and the deadrise angle are systematically varied.

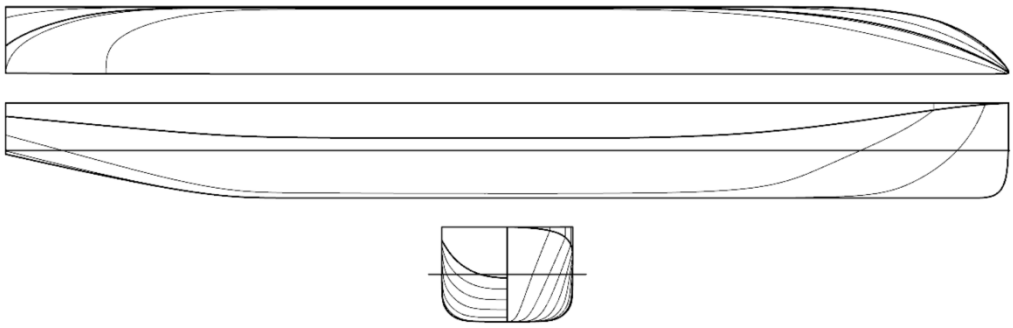


Figure 3 Lines plan for the Ecoliner Parent hull.

Table 1 Main particulars for the Ecoliner Parent hull.

	Full Scale	**Model Scale (α = 50)**
LOA	138 m	2.76 m
Beam	18 m	0.36 m
Draft	6.5 m	0.13 m
Displacement	11,896 ton	92.8 kg
C_P	0.719	0.719
C_P	0.764	0.764
C_M	0.942	0.942
LCB	50.13 %	50.13 %
Wetted Surface	3,293 m^2	1.312 m^2

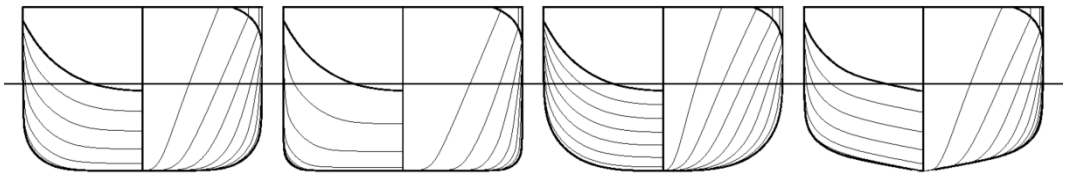


Figure 4 Bare hull validation cases (from left to right): Hull 1 – Bare (parent), Hull 16 – Bare (C_P^+ C_M^+), Hull 19 – Bare (C_P^- C_M^-), and Hull 34 – Bare (10^o $deadrise$).

The variation for prismatic coefficient is effected by lengthening or shortening the parallel mid-body. The midship coefficient is modified by increasing and decreasing the bilge radius. For variations in the draft-to-length ratio, the displacement is kept constant by reducing the beam accordingly. Finally, the deadrise hulls are defined by extending a tangent line from the bilge to the centreline at the appropriate angle.

Table 2 Summary of the Delft Wind-Assist Series.

Hull	C_P	C_M	T/L	Deadrise
1 $(parent)$	0.764	0.942	0.047	0^0
16 $(C_{\mathrm{P}}^{+}\ C_{\mathrm{M}}^{+})$	0.840	0.984	0.047	0^0
19 $(C_{\mathrm{P}}^{-}\ C_{\mathrm{M}}^{-})$	0.689	0.874	0.047	0^0
34 $(10^o\ deadrise)$	0.764	0.838	0.047	10^0
$DWA\ Series\ Min$	0.686	0.787	0.042	0^0
$DWA\ Series\ Max$	0.840	0.984	0.060	14^0

The extents of the systematic series and the geometry for validation cases are presented in Table 2. Hull 1 and Hull 34 were selected as representative hulls for the series; Hull 1, being the parent hull at the centre of all variations, and Hull 34 as the median case for the deadrise hulls. Hull 16, with sharp bilges, is expected to generate pronounced bilge vortices, challenging the capabilities of the fluid modelling in this respect. Hull 19, with a slender form and rounded bilges, will challenge the modelling for flow separation. Together, the validation set is considered to well-represent the entire Delft Wind-Assist systematic series. It is assumed that a favourable result for the validation set can be interpreted as a validation statement for the series as a whole.

2.2 APPENDED GEOMETRIES

Hull 1 and Hull 34 were fitted with a series of appendages that was designed to represent a broad range of appendage typologies. Hull 1 was fitted with a Rudder and Bilge Keels. The rudder was mounted on a high-precision quadrant that could be set to 0°, -6°, and +6°. Hull 34 was fitted with a Skeg and a combination Skeg and Barkeel.

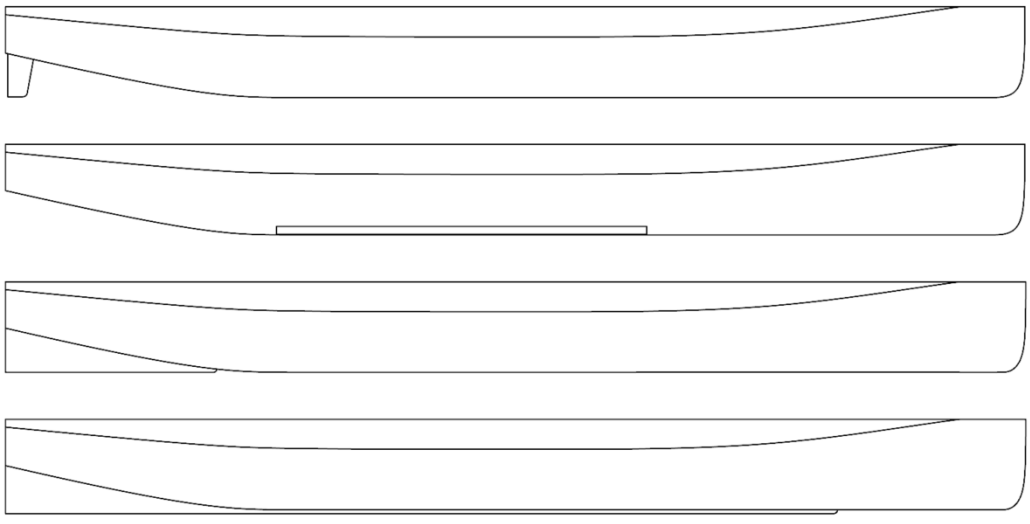


Figure 5 Overview of appended validation cases (from top to bottom): Hull 1 - Rudder, Hull 1 - Bilge Keels, Hull 34 - Skeg, Hull 34 - Skeg + Barkeel.

2.3 EXPERIMENTAL CAMPAIGNS

The validation data used in this exercise was collected during two experimental campaigns, in 2015 and in 2016. Hull 1 – Bare, Hull 16 – Bare, and Hull 19 – Bare were tested during the 2015 campaign (Struijk, 2015). Hull 34 – Bare and all appended cases were tested in 2016. With the intent to eventually make statements about the validation level of simulations, it is necessary to address any inconsistencies in the validation data set, especially as may pertain to the experimental uncertainty. Two items need to be addressed: the treatment for sinkage and trim, and the adoption of a uniform strip resistance coefficient. During the 2015 experiments, the model was mounted using the setup normally used for sailing yachts at Delft University of Technology (Keuning & Sonnenberg, 1998): free to trim and sink according to the speed and leeway angle. A fully restrained setup was used during the 2016 experiment, with trim and sinkage both set to zero. All simulations were performed with heave and pitch constrained. In view of the low Froude numbers considered, a large discrepancy is not expected. No correction to the experimental data was made for trim or sinkage. The motivation for this change will be discussed further in Section 4. Finally, a uniform turbulence stimulation resistance coefficient, C_{TS}, was adopted, determined in 2016 for Hull 34. The post-processing for the 2015 experiment was revisited with the 2016 C_{TS} value.

3 VALIDATION METHODOLOGY

Fluid flow around the sailing ship will experience separation effects and will become entrained in large vortices in the wake of the ship. As discussed in the introduction, the modelling of these phenomena is the principal simulation challenge.

3.1 VALIDATION STATEMENT

The methodology for validation is taken from the International Towing Tank Conference (ITTC) guideline (ITTC, 2014) and from the American Society of Mechanical Engineers (ASME) standard (ASME, 2009). A validation statement is made according to the relationship between the comparison error, defined as the difference between simulation and experimental values: $E = Sim - Exp$, and the validation standard uncertainty, u_{Val}, which is a combination of the uncertainties associated with the simulation and experimental data.

The following validation statement is adopted from (ITTC, 2014):

$|E| < u_{\mathrm{Val}}$: The comparison error falls within uncertainty band defined by validation standard uncertainty. The modelling error is within the 'noise level' of the validation exercise. The simulation is validated with a validation level equal to u_{Val}.

The validation level, u_{Val}, is of interest as a measure of the uncertainty of simulation data. If the validation statement is affirmative, confidence commensurate with the validation level is placed

on the simulation methodology. This estimate of the uncertainty for simulation data is retained for further work in regression analysis.

One objective of this validation exercise is to bound the modelling errors with a bandwidth defined by the validation standard uncertainty:

$$\delta_{\mathrm{Model}} \in [E - u_{\mathrm{Val}}\,, E + u_{\mathrm{Val}}] \qquad (1)$$

The modelling error may be inferred from the results of the validation exercise without making assumptions about the probability distribution of the errors $\left(\delta_{Num} + \delta_{Input} - \delta_{Exp}\right)$ if the magnitude of the comparison error is (much) larger than the validation level:

$$|E| \gg u_{\mathrm{Val}} \qquad (2)$$

In which case $\delta_{Model} \approx E$. Otherwise, the modelling error is obscured by the 'noise level' of the validation exercise, represented by u_{Val} (ASME, 2009).

Determining u_{Val} is thus a central task in the validation exercise. Following the derivation from the ASME standard, the error for a simulation result is separated into a component arising due to the modelling assumptions and approximations (δ_{Model}), and a component arising from the numerical solution of the equations, (δ_{Num}). Input uncertainties are excluded in this exercise. The numerical error is expressed as an uncertainty, U_{Num} (Roache, 1997) (Eça & Hoekstra, 2014). Assuming U_{Num} and U_{Exp} are uncorrelated, and neglecting U_{Input}, the following definition is adopted:

$$u_{\mathrm{Val}} = \sqrt{{U_{\mathrm{Num}}}^2 + {U_{\mathrm{Exp}}}^2} \qquad (3)$$

An example of a model error, and a central complication for the validation data, is the possible effect of the turbulence stimulators on separation location and on the strength of any separated vortices (as determinants for the sideforce and yaw moments). In this case, one might argue that the simulation better resembles a real ship. However, the validation exercise measures the degree to which the simulation is able to reproduce experiments and the fault is therefore a modelling error for the simulation. Similarly, vessel sinkage and trim, which was allowed during the 2015 experiments and constrained for the 2016 experiments, is constrained for all simulations. Although the 2016 experiment is less realistic, one component of the simulation modelling error has been removed. The focus here is the test the capabilities of RANS-CFD for separating flow structures, and the validation cases might better be thought of as ship-like forms. An unambiguous categorization of numerical and the modelling errors is necessary to isolate and quantify the modelling error.

The validation procedure is carried out without modification for the case for $Fn = 0.17$ and $\beta = 0°$, 6°, 9°, for which an estimate for the validation standard uncertainty is directly available. These results are presented in Section 6.

3.3 EXTENDED VALIDATION STATEMENT

A validation statement is made for simulation of the Delft Wind-Assist Series by applying a multivariate validation metric as proposed in (Hills, 2006) to the validation data set. It is assumed that the validation exercise and the statistics for the comparison error of the validation cases will be representative of the entire wind-assist series. The multivariate metric compares the radius of a hyper-ellipse defined by the set of validation points with a reference radius for a corresponding normal distribution. The radius r and r_{ref} are defined (Hills, 2006):

$$r = \sqrt{\mathbf{E}^T \boldsymbol{V}_{Val}^{-1} \boldsymbol{E}} \qquad (4)$$

$$r_{ref} = \sqrt{N + \sqrt{2N}} \qquad (5)$$

$\boldsymbol{E}$ is the vector of N comparison errors, and $\boldsymbol{V_{Val}}$ is the covariance matrix, a diagonal matrix with the squared validation uncertainty for each validation point along the diagonal. If the ratio r/r_{ref} is larger than one, than the comparison errors are generally larger than the validation level. For r/r_{ref} less than one, the errors are less than expected for the corresponding normal distribution with N degrees of freedom. Following the same argumentation as for the single-point validation statement above, the simulation is regarded as validated for r/r_{ref} less than one, with a validation level according to the values for u_{Val}.

4 EXPERIMENTAL METHOD

4.1 EXPERIMENTAL SETUP

Experiments were designed to obtain validation data with minimal uncertainty. As detailed in Section 2, the validation data was collected during two experimental campaigns, in 2015 and 2016. The setup for the experiment was altered for the 2016 campaign. The fully constrained setup, with the six-component measurement frame, rather than the sailing yacht set-up, gave better control over the position of the model, and provides extra flexibility when designing the arrangement of sensors; again with the aim to minimize experimental uncertainty. The 2016 experiments are described in the remainder of this section. The yacht setup of the Delft Ship Hydromechanics laboratory is documented in (Keuning & Sonnenberg, 1998).

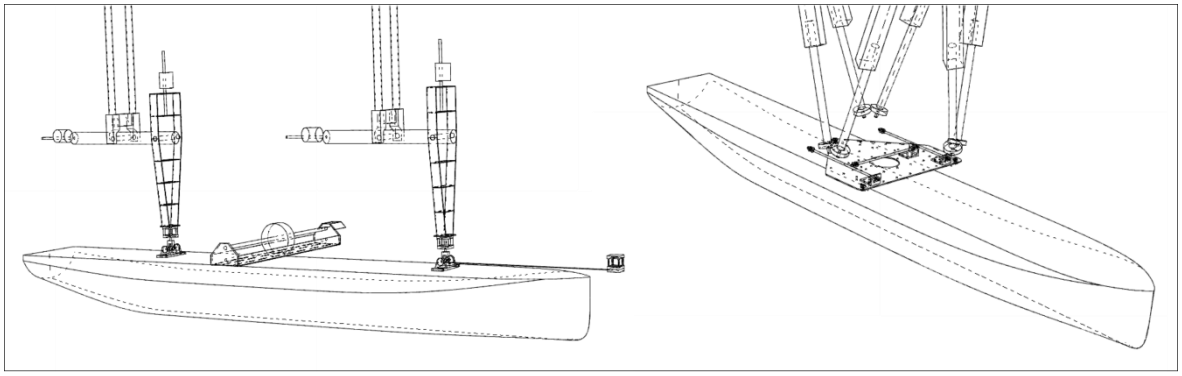


Figure 6 Sailing yacht experimental setup for 2015 campaign (left) and hexapod for 2016 campaign (right).

During the 2016 test campaign, the models were tested in fully captive setup. The models were connected to the hexapod with the six-component measurement frame. The measurement frame is designed to resolve any applied force or moment into orthogonal forces and moments. The hexapod setup is illustrated in Figure 6 (right), with the top plate of the six-component frame removed for clarity. The arrangement of the sensors on the measurement frame was made to obtain the best possible fidelity for the sideforce. The position of the model is recorded using a Certus optical tracking system. All signals are filtered with a low-pass filter set to 100 Hz before sampling to prevent aliasing. The signal is sampled at a frequency of 1000 Hz and written to disc.

The measurement campaign was three weeks long. To assure that a consistent procedure was followed, the following protocol was adopted:

1) Model set to zero leeway position for nul measurement.
2) Model set to leeway angle for second nul measurement.
3) Carriage accelerated to test speed. 10 seconds is allowed for the flow to reach a steady condition.
4) Measurements recorded for 60 seconds.

The nominal rest period between runs was 20 minutes. The test program is arranged so that high-speed runs and repeat runs were interspersed regularly, and so that a low-speed run did not immediately follow a high-speed run. The first run of each day, and the first run after a weekend, was marked in the measurement log.

4.1.1 Turbulence Stimulators

The models were fitted with turbulence stimulators to ensure a turbulent boundary layer along the hull. The correction for an added resistance due to turbulence stimulation was determined according to the standard practice of the Delft Ship Hydromechanics Laboratory by comparing resistance curves obtained for single- and double strip configurations. The turbulence stimulation strip resistance coefficient was determined for Hull 34 - Bare. This value is adopted for all other data, including results from the 2015 experiment. The resistance is corrected for the change in resistance due to the presence of turbulence stimulators:

$$\Delta R_{TS} = \frac{1}{2}\rho V^2 C_{TS} A_{TS} \quad (6)$$

A_{TS} is the area of the turbulence stimulator.

4.1.2 Bow Wave Measurements

As a further qualitative check for the simulations, the interface capturing for the asymmetric bow wave was compared to measurements from experiments. The profile of the bow wave was measured using cameras and grid markings on the ship. The images were de-warped to correct for lens effect and perspective and scaled so that one is pixel was equal to 0.5 mm. It was then possible to measure the position of the maximum and minimum wave elevation. This exercise was performed for Hull 34 – Bare.

4.2 EXPERIMENTAL UNCERTAINTY

The experimental uncertainty is determined according to the ITTC guideline for planar motion tests (ITTC, 2014). The following error components were found to be significant: bias errors arising from the measurement of forces and moments with the six-component frame, bias errors arising from model misalignment in the tank, bias errors due to geometric faults in the model construction, and an end-to-end estimate of the precision error for the complete experimental setup. The calculation of U_X is detailed for Hull 34 - Bare at $Fn = 0.17$ and $\beta = 9^0$.

4.2.1 Bias Errors

It is necessary to determine the sensitivity for each force component to each bias error. The standard manoeuvring non-dimensionalization is used to derive the sensitivities, defined as the partial derivative with respect to the quantity of interest:

$$X' = \frac{X}{\frac{1}{2}\rho U^2 TL} \quad (7)$$

$$\frac{\partial}{\partial F_X} X' = \frac{2}{\rho U^2 TL} \quad (8)$$

$$\frac{\partial}{\partial \beta} X' = X'_\beta \quad (9)$$

$$\frac{\partial}{\partial T} X' = \frac{-2F_X}{\rho U^2 T^2 L} \quad (10)$$

The bias error for forces measured with the six-component frame was estimated by repeating the calibration process for the fully assembled frame. The six-component measurement frame contributes to the stiffness of the measurement system. A variety of forces and moments were applied to the frame, giving a correction to the calibration for X, Y, and N of 0.5%, 1.2%, and -1%, respectively. The remaining disparity, including a significant hysteresis effect, was used as B_{F_X}. The hysteresis phenomena observed for strain gauges is exacerbated for the mechanically complex measurement frame. Anticipating that the vibrations of a moving carriage would

encourage a settling of the frame, a set of measurements was made with a typical carriage speed. In fact the hysteresis effect was significantly reduced. The estimate for B_{F_X} is therefore likely a conservative value.

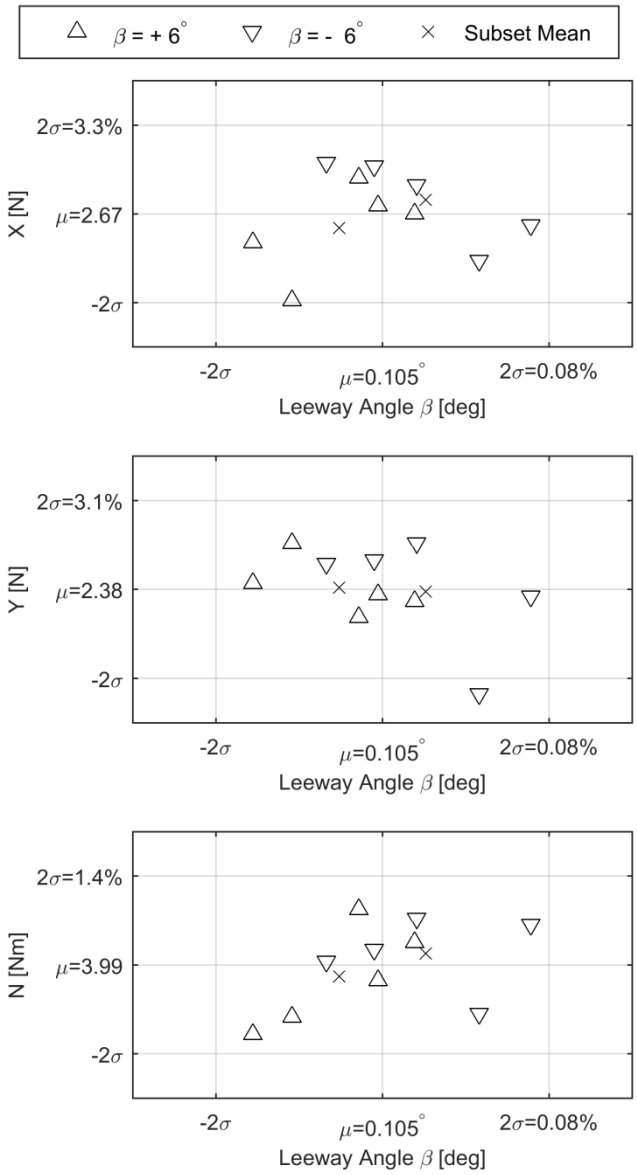


Figure 7 Bias estimate for alignment of Hull 1 – Rudder. Measured forces for positive and negative angles are presented together, demonstrating the symmetry of the experimental setup.

The alignment of the model for each case was measured with ten repeat runs, with five positive leeway angles and five negative leeway angles. This allowed for a test for the symmetry of the system and also gave an indication for the precision of the setup. These runs were arranged so that the position of the model was changed before each run, i.e., the model was not simply towed repeatedly for a single condition. For Hull 1 – Rudder, the rudder angle was set to positive and negative angles (five runs with +6° leeway, +6° rudder, and five runs with -6° leeway, -6° rudder) as in Figure 7. These runs were interspersed throughout the measurement campaign so that the

ship position and rudder angle were altered before each repeat run. The bias error for leeway angle, B_β, was estimated using the x-intercept of the linear fit for these results. As a conservative estimate, a sum was made of the absolute offset determined using the sideforce and the yaw moment. This estimate for the bias might also contain the influence of an asymmetry in the model geometry. Finally, the bias error due to faults in the model geometry is assumed $B_\mathrm{T} = 1.5$ mm.

The bias error for X is expressed as an expanded uncertainty with 95% confidence level (ITTC, 2014).

$$B_\mathrm{X} = 2\sqrt{\left(\frac{\partial X'}{\partial F_\mathrm{X}}\right)^2 B_{F_\mathrm{X}}^2 + \left(\frac{\partial X'}{\partial \beta}\right)^2 B_\beta^2 + \left(\frac{\partial X'}{\partial T}\right) B_\mathrm{T}^2} \qquad (11)$$

4.2.2 Precision Errors

The repeatability of the measurement is an "end-to-end" test for the precision of the setup. The repeat runs are meant to capture any variations in the test condition over the duration of the test program. Ten repeat runs (positive leeway angle only) were carried out for Hull 34 – Skeg, and the precision of the setup was determined as:

$$P_X = 2.228 * \sigma_X \qquad (12)$$

Table 3 Details for calculation of experimental uncertainty for Hull 34 – Bare at $\boldsymbol{Fn}$=0.168 and leeway angles $\boldsymbol{\beta}$= 9°, for $\boldsymbol{X}$. The uncertainty $\boldsymbol{u'}$ is given as a percentage of the measured value. The precision error is the dominant term.

$\boldsymbol{\Theta}$	$\frac{\partial F_X}{\partial \Theta}$	$\boldsymbol{\delta_\Theta}$	$\boldsymbol{u_\Theta}$ **[N]**	$\boldsymbol{u'_\Theta}$ **[%]**
F_X	0.014	0.0243 N	0.047	1.8%
β	0.012	0.17^0	0.010	0.4%
T	0.29	0.0015 m	0.059	2.3%
P	-	-	0.120	4.6%

The uncertainties are combined as uncorrelated quantities:

$$U_X = \sqrt{{B_X}^2 + {P_X}^2} \qquad (13)$$

6 RESULTS & DISCUSSION

The results for the validation exercise are presented. The direct validation for Hull 1 – Bare at $\boldsymbol{Fn}$=0.168 and leeway angles $\boldsymbol{\beta}$= 0°, 6°, 9° is given. The validation statement is made for the bare-hull geometries in the Wind-Assist Series, followed by the visualization of the bow wave profile for Hull 34 – Bare. Finally, results for the validation of select appended geometries are given.

6.1 EXPLICIT VALIDATION CASE

All components of the validation standard uncertainty are available for Hull 1 – Bare at $Fn = 0.168$ and for leeway angles β= 0°, 6°, 9°. The mesh contains 6M cells, requiring four hours to perform one simulation with the available computing resources.

Table 4 Validation for Hull 1 – Bare.

	U_{Exp}	U_{Num}	u_{Val}	E	u_{Val} [%]	E [%]
$Fn = 0.168$, β= 0°						
X	0.080 N	0.140 N	0.180 N	0.026 N	7.6 %	1.67 %
$Fn = 0.168$, β= 6°						
X	0.117 N	0.107 N	0.166 N	0.034 N	6.4 %	1.42 %
Y	0.0888 N	0.133 N	0.157 N	-0.005 N	11.9 %	-0.37 %
N	0.251 Nm	0.336 Nm	0.422 Nm	-0.074 Nm	8.3 %	-1.46 %
$Fn = 0.168$, β= 9°						
X	0.124 N	0.227 N	0.268 N	0.028 N	9.3 %	1.08 %
Y	0.126 N	0.137 N	0.189 N	-0.080 N	8.0 %	-3.39 %
N	0.350 Nm	0.347 Nm	0.495 Nm	0.117 Nm	6.7 %	1.59 %

A very good agreement between the simulation result and the experimental value is reported in Table 4. The comparison error is less than the validation uncertainty for all cases, and the simulation is validated at the respective validation levels. The experimental and numerical uncertainties are of similar magnitudes. Details for the comparison error and the validation level are presented in Table 4.

6.3 BOW WAVE PROFILE

The bow wave elevation was measured with cameras and using grid markings on the model. A formal validation statement is not possible as the uncertainty associated with the simulation waterline was not determined. A good quantitative agreement is reported for the maximum bow wave height and location (pressure side), and the minimum wave height and location (suction side). The distance between the simulation and experimental value is reported as $\delta = \sqrt{\delta_x + \delta_y}$. The median error values occurred for $Fn = 0.168$ and $\beta = 6^0$. For this case, the error for the bow wave crest (pressure side) is δ=4.6 mm. The error for the bow wave trough (suction side) is δ=5.0 mm. The results for this case are shown in Figures 8 and 9.

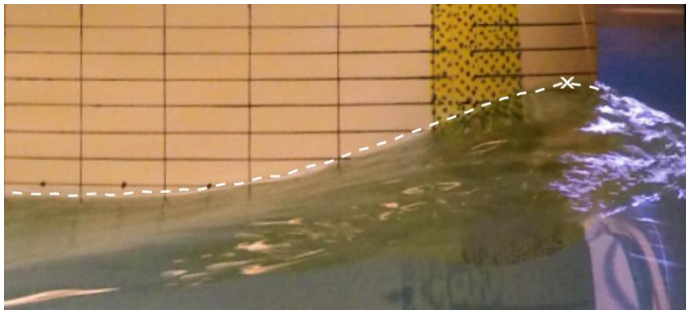


Figure 8 Pressure side bow wave profile corresponding to the median error (Fn=0.168 and β=6^0). The image has been overlaid with the wave elevation obtained by simulation.

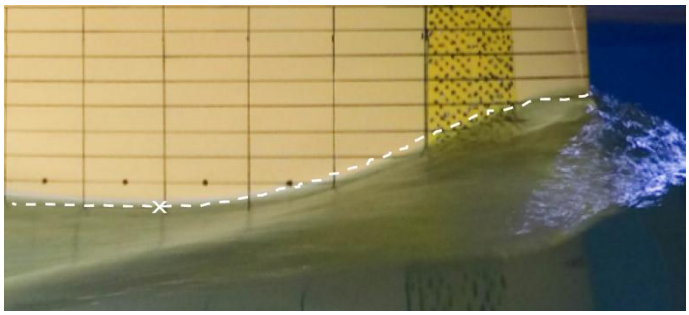


Figure 9 Suction side bow wave profile corresponding to the median error (Fn=0.17 and β=6^0). The image has been overlaid with the wave elevation obtained by simulation.

6.4 VALIDATION STATEMENT FOR RANS-CFD SIMULATION OF THE DELFT WIND-ASSIST SERIES

As described in Section 3.3, the ratio r/r_{ref} is adopted as a multiple-point validation metric. There are three validation points (resistance X, sideforce Y, and yaw moment N) for each hull at each operating condition, or 120 validation points in total. Results for r/r_{ref} are also presented per force component. Several assumptions are required for the numerical uncertainty, which is only available for the parent hull (Hull 1), at $Fn = 0.168$ and for leeway angles β= 0°, 6°, 9°. The computational effort required to determine the numerical uncertainty for additional geometries and operating conditions was prohibitive. The numerical uncertainty for the sideforce in particular may be the dominant contribution to the validation level. Results for r/r_{ref} are presented for several subsets of the validation data set, defined according to the assumptions made for the numerical uncertainty. Subset 1 is defined by cases where the numerical uncertainty is directly available, for $Fn = 0.168$ and for leeway angles β= 0°, 6°, 9°. Subset 2 consists of all hulls of the bare-hull validation set at the same operating condition as Subset 1, where it is assumed that the numerical uncertainty is unchanged for varying hull geometry. Finally, r/r_{ref} is given for the complete validation set ($N = 120$). Here it is assumed that the numerical uncertainty at $Fn = 0.168$ and leeway angle β= 3° is equal to the uncertainty at $Fn = 0.168$ and β= 6°. The numerical uncertainty at other speeds in the validation data is assumed to scale with the magnitude of the measured quantity.

Table 5 Validation level $\boldsymbol{u_{Val}}$ for Hull 1 – Bare.

Speed/Leeway	$\boldsymbol{u_{Val}}$: $\boldsymbol{X}$	$\boldsymbol{u_{Val}}$: $\boldsymbol{Y}$	$\boldsymbol{u_{Val}}$: $\boldsymbol{N}$
Fn=0.128, β= 0°	0.103 N (7.8%)	-	-
Fn=0.128, β= 3°	0.094 N (6.8%)	0.089 N (28.8%)	0.189 N (13.8%)
Fn=0.128, β= 6°	0.096 N (6.6%)	0.099 N (13.7%)	0.238 N (8.5%)
Fn=0.128, β= 9°	0.150 N (9.4%)	0.117 N (9.0%)	0.282 N (7.0%)
Fn=0.168, β= 0°	0.180 N (7.7%)	-	-
Fn=0.168, β= 3°	0.161 N (6.6%)	0.148 N (25.2%)	0.372 N (14.0%)
Fn=0.168, β= 6°	0.166 N (6.4%)	0.157 N (11.9%)	0.423 N (8.3%)
Fn=0.168, β= 9°	0.268 N (9.3%)	0.189 N (8.0%)	0.495 N (6.7%)
Fn=0.21, β= 0°	0.310 N (7.6%)	-	-
Fn=0.21, β= 3°	0.276 N (6.5%)	0.229 N (23.5%)	0.587 N (13.4%)
Fn=0.21, β= 6°	0.281 N (6.3%)	0.249 N (11.8%)	0.665 N (8.2%)
Fn=0.21, β= 9°	0.452 N (9.3%)	0.305 N (7.9%)	0.791 N (6.6%)

The ratio r/r_{ref} must be considered against the validation uncertainty, which form the entries of the covariance matrix V_{Val}. The validation uncertainty for Hull 1 – Bare is presented in Table 5 in absolute and relative terms. The validation uncertainties for other geometries will vary as the experimental uncertainty can be computed for all cases, but the values for Hull 1 – Bare are representative. The magnitude of the sideforce at low speeds and for small angles is such that the validation uncertainty, when expressed in relative terms, may exceed 25%.

The simulation data to be obtained for hulls in the Delft Wind Assist series will be evaluated in subsequent analysis together with a confidence interval dictated by this validation exercise. Although a detailed discussion of the derived quantities used for modelling for wind-assist vessels is outside the scope of this publication, this material is briefly introduced to highlight the implications of the validation levels presented. See: (Keuning & Sonnenberg, 1998) and (van der Kolk, 2016). The principal quantities of interest for are the increase in resistance due to sideforce production, X_i, and the centre of effort for hydrodynamic sideforce, CoE, which is related to the maneuverability of the sailing vessel.

$$X_i = X - X_{\beta=0^\circ} \tag{14}$$

$$\mathrm{CoE} = {}^{N}/_{Y} \tag{15}$$

The resistance increase due to sideforce production is modelled as an effective draft T_e, representing the efficiency of the hull. This quantity is related to the slope of a linear fit through data for several leeway angles. The second quantity of principal interest for this modeling for wind-assist vessels is the center of effort (CoE) for the distribution of lateral force, which is related to the manoeuvrability of these vessels. The position of the CoE is determined as the quotient of the yaw moment and the sideforce. The implications of the validation levels presented here for these derived quantities will be discussed below.

Table 6 Details of the validation for the Delft Wind-Assist series.

	All	***X***	***Y***	***N***
Hull 1, $Fn = 0.168$, β= 0°, 6°, 9°				
$\boldsymbol{r/r_{ref}}$	0.17	0.17	0.14	0.13
All hulls, $Fn = 0.168$, β= 0°, 6°, 9°				
$\boldsymbol{r/r_{ref}}$	0.60	0.39	0.73	0.58
Complete validation set				
$\boldsymbol{r/r_{ref}}$	0.59	0.30	0.84	0.45

Results for simulation validation for the complete Wind-Assist Series are presented in Table 6. The multiple set-point validation metric r/r_{ref} is less than one for all subsets and all entries, meaning that the comparison errors are generally less than the associated uncertainties. Following the validation approach outlined in Section 3, the simulation method for the Delft Wind-Assist Series is validated at the validation levels summarized in Table 5. $r/r_{ref} \ll 1$ for all entries for the first subset indicates that the comparison error for these cases is much less than the associated validation uncertainties. This is the same result already presented as a point-wise validation in Table 4. The simulation results for Hull 1, at these operating conditions, are in very close agreement with the validation data.

Simulation and experimental results for resistance, sideforce, and yaw moment are presented in Figures 10 – 13 for the validation set with $\beta \neq 0°$. The distribution of comparison errors is presented in Figure 14. The comparison errors for each component, for each operating condition and for each hull follows, for which the validation level presented in Table 5 must be kept in mind.

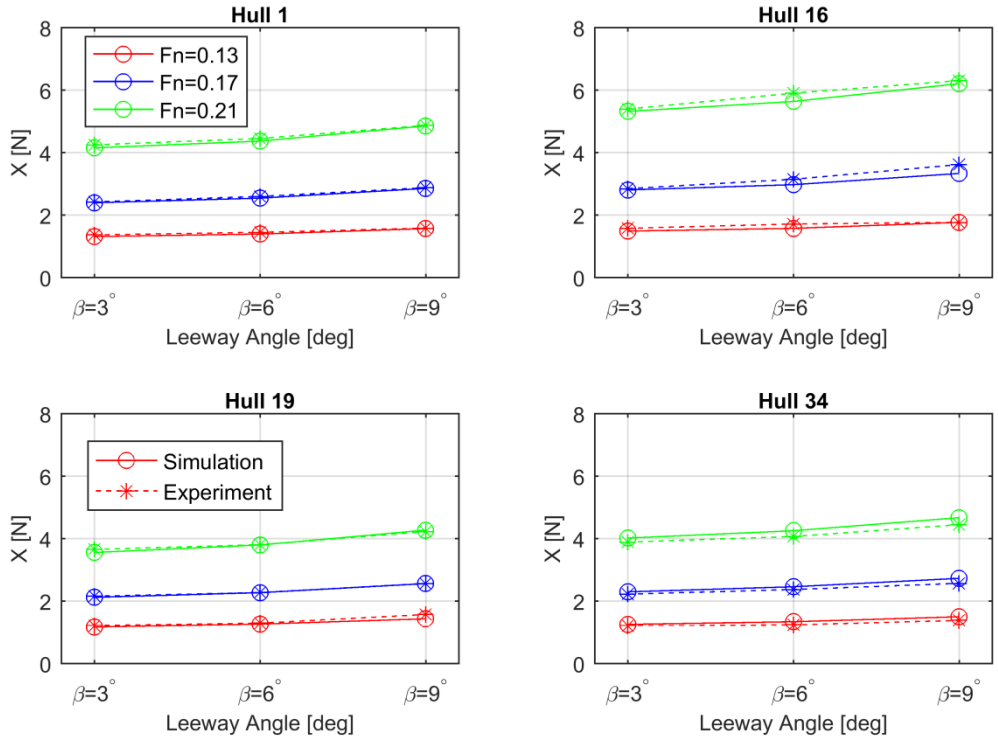


Figure 100 Simulation and experimental results from the bare-hull validation set for resistance.

Simulation and experimental values for resistance are presented in Figure 10. With the exception of Hull 16, excellent agreement between these data is observed. Resistance for Hull 16, the fuller hull with small bilge radius, is under-predicted, though the comparison errors do lie within bounds of the validation level (r/r_{ref}=0.62 for resistance for Hull 16).

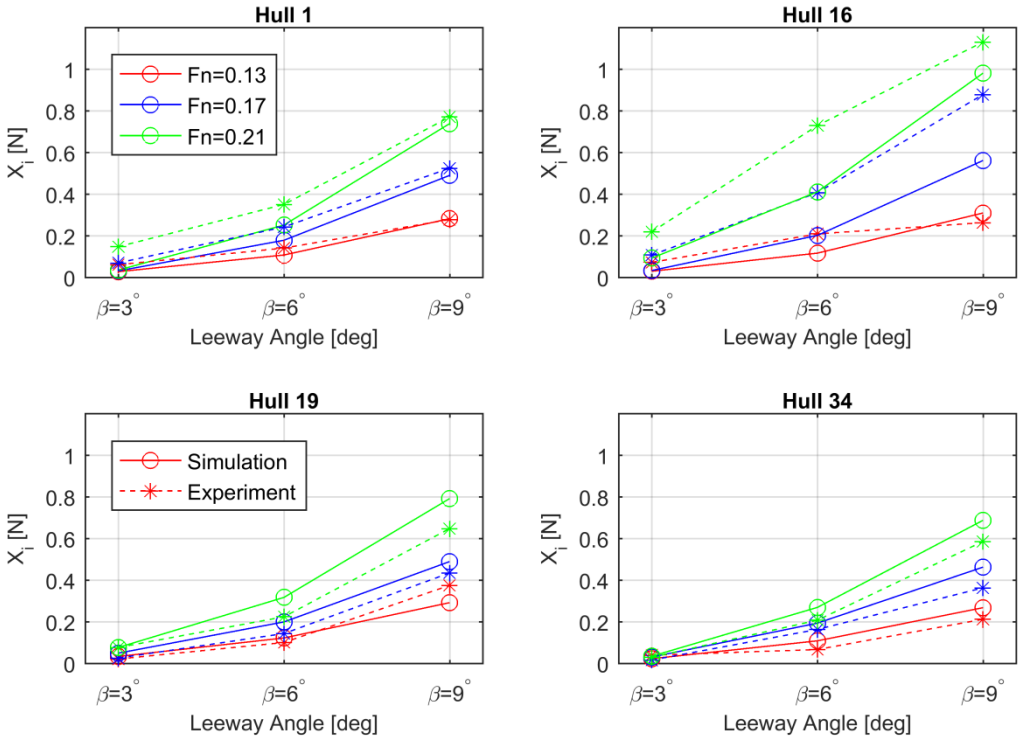


Figure 11 Simulation and experimental results from the bare-hull validation set for resistance due to leeway.

For modelling of wind-assist vessels, the resistance increase due to sideforce, X_i, is the relevant quantity. This derived quantity is determined from simulation and experimental values and presented in Figure 11. This quantity is approximately one order-of-magnitude smaller than the data used for this validation exercise. The validation uncertainty for resistance, when expressed as a percentage of X_i, lies between 25% and 200% (without considering the combination/ correlation of errors for the values $X_{\beta=0°}$, X). Still, a good agreement for the trends in this data is observed, considering the order-of-magnitude of the data and the uncertainties present. The comparison between simulation and experimental results is poorest for Hull 16, the fuller hull with small bilge radius. Stronger separation behaviour at the bilge and a larger, more energetic wake of vortices is expected for this hull, and the simulation is apparently unable to capture the behaviour completely. In subsequent analysis for the derivation of a regression model for wind assist vessels, the efficiency of a hull is expressed as an effective draft T_e. This quantity is related to the slope of a linear fit through data for several leeway angles. The data at 9° leeway (for maximum X_i) where the validation level for resistance is approximately 25% of X_i, is sufficient to determine the effective draft of the vessel. Though the magnitude of X_i is quite small compared to the uncertainties present for resistance, the linear modelling for the effective draft T_e permits an analysis that relies on the larger values only, for which the validation level is no longer prohibitive.

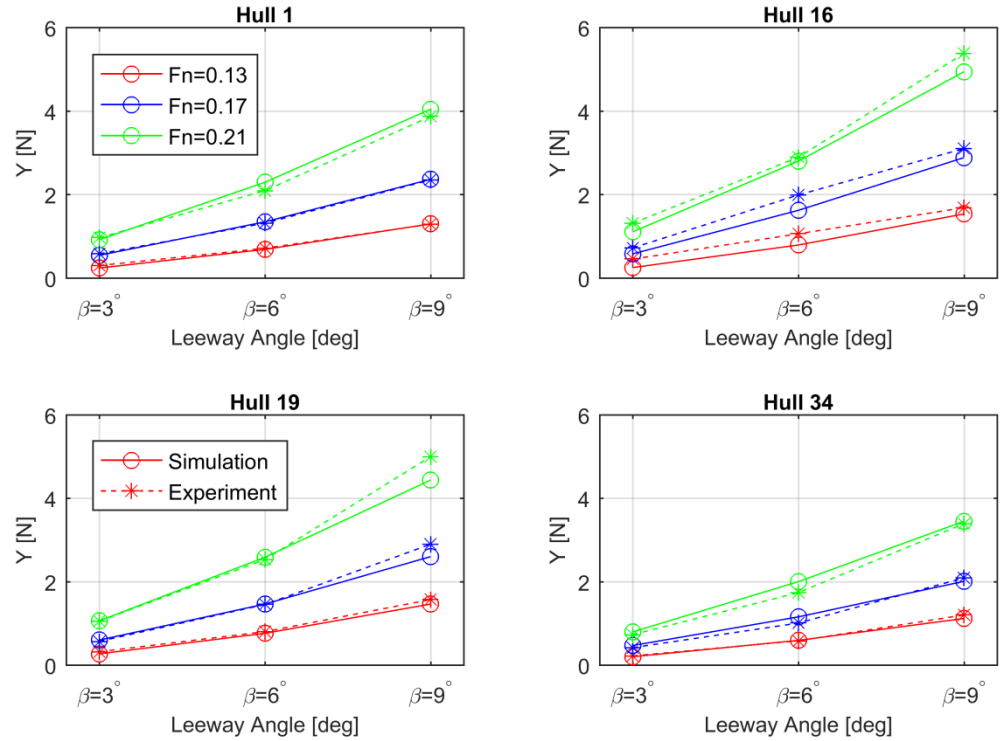


Figure 12 Simulation and experimental results from the bare-hull validation set for sideforce.

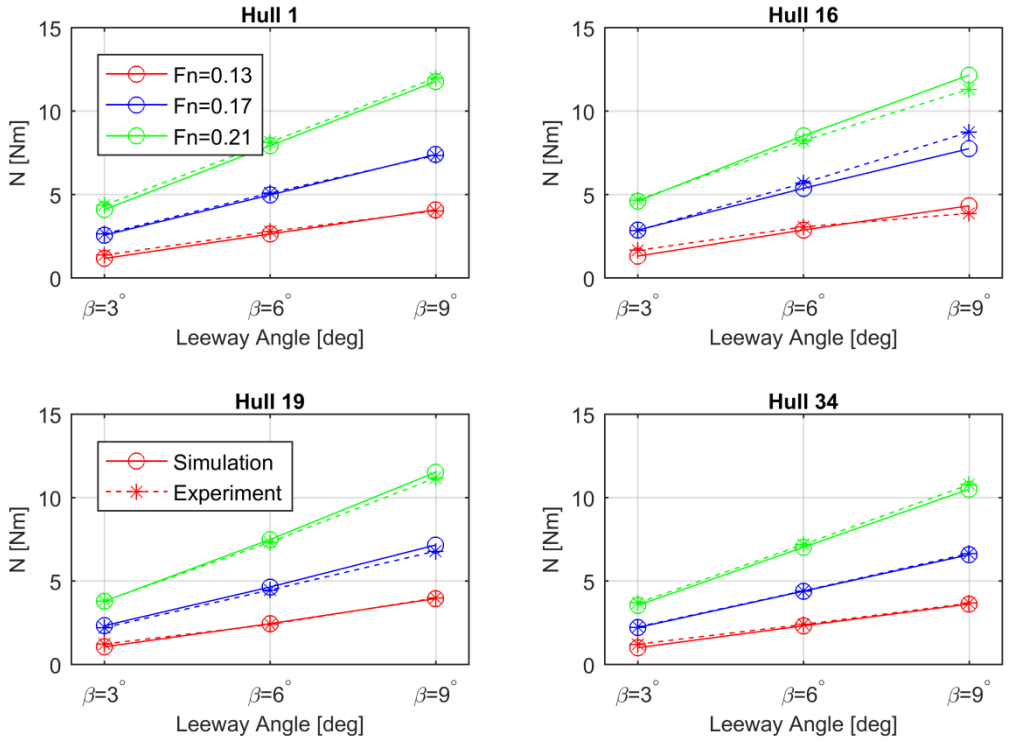


Figure 13 Simulation and experimental results from the bare-hull validation set for yaw moment.

Results for sideforce and yaw moment presented in Figure 12 and Figure 13 show close agreement, with the exception of the sideforce for Hull 16. Here again, a consistent under-

prediction is observed for the hull where strong separation behaviour is expected. As discussed above, it is likely that logarithmic wall modelling is inadequate for the separation behaviour associated with cross-flow drag, a sideforce component that should be quite strong for this hull. For reference, r/r_{ref}= 1.26 for sideforce Y for Hull 16. This appears to be a systematic error for all operating cases, raising the possibility of implementing a correction for the simulation value. For context, the comparison error is on average 33% larger than the validation level for this hull. In contrast with the sideforce, the comparison error for yaw moment for Hull 16 is much smaller, yielding an r/r_{ref}= 0.68. A wall-resolved boundary layer modelling may be a more appropriate simulation approach, but the computational cost is deemed prohibitive in light of the volume of simulations anticipated.

The second quantity of principal interest for this modeling for wind-assist vessels is the center of effort (CoE) for the distribution of lateral force, which is related to the course-keeping ability of these vessels. The position of the CoE is determined as the quotient of the yaw moment and the sideforce. The yaw moment is well-predicted by simulation, but the validation level for the sideforce is similarly troubled as the induced resistance above. For the sideforce, the large contribution of the numerical uncertainty (see Table 4) is a compounding factor. Despite the large (relative) uncertainties associated with the prediction sideforce production, the results presented in Figure 12 show a good agreement between simulation and the validation data. Even for Hull 16, a consistent offset is observed, but it may be said that the trend in the validation set is reproduced by simulation.

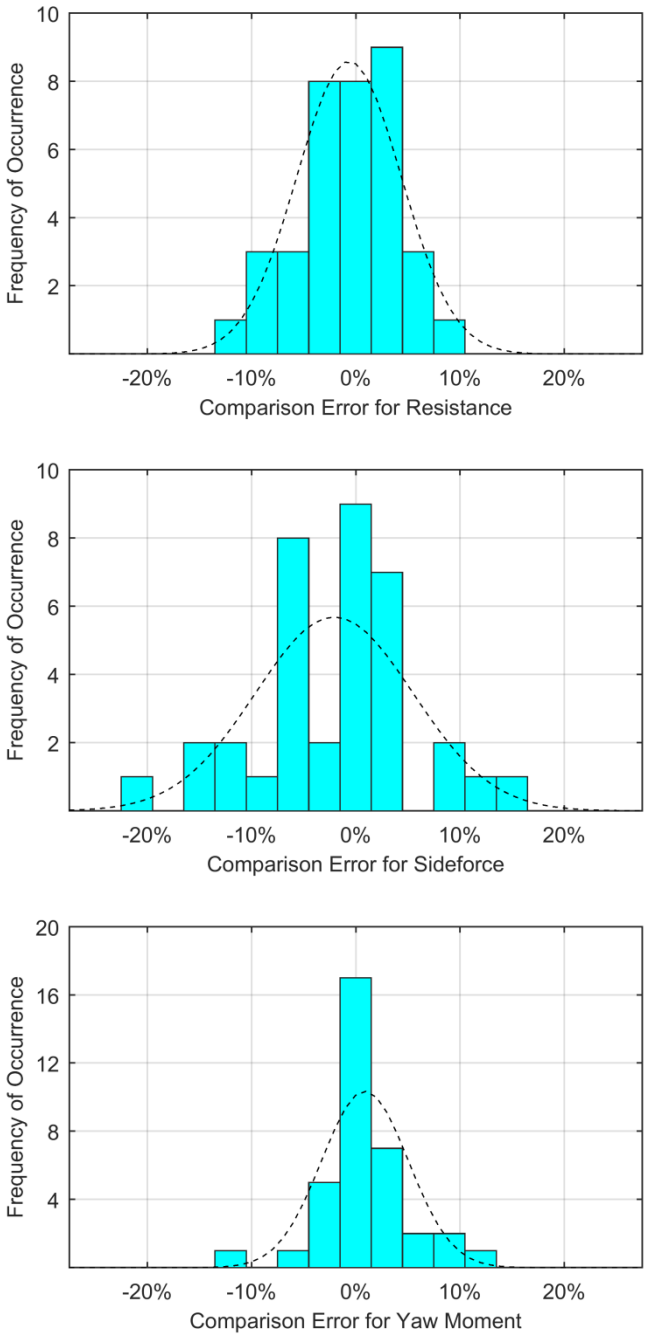


Figure 14 Distribution of comparison error for the of bare hull validation cases $\boldsymbol{\beta \neq 0}$° (N=36).

The distribution of comparison errors is presented in Figure 14 for cases where the leeway angle $\beta \neq 0°$. Resistance runs at $\beta = 0°$, a routine application of RANS-CFD, were excluded to create a data sets with the same number of entries (N=36) for resistance, sideforce, and yaw moment. The comparison error is made relative using a constant equal to one half of the range of the measurands:

$$E_{\text{Ens}} = (100) * \frac{Sim - Exp}{\frac{1}{2}(max(Exp) - min(Exp))} \qquad (16)$$

This definition for an ensemble comparison error was adopted to facilitate the presentation of the entire validation set as a distribution of relative errors. It is a compromise that attempts to accommodate the range in order-of-magnitude for the sideforce and yaw moment by scaling the comparison error approximately in proportion with the validation uncertainty. If each error is expressed as a percent of the experimental value, errors that do not scale with the measurand would be overstated for smaller values of sideforce and yaw moment. Under the present definition of an ensemble comparison error, E_{Ens}, the normalisation by a constant value for all errors will understate the relative error for small values of sideforce and yaw moment and overstate the relative errors for large values. For small values of sideforce, the validation level is larger in percentage terms, motivation the suppression of these errors. The opposing tendency exists for larger measurands.

Table 7 Statistics for distribution of comparison errors.

	$\mu_{\mathbf{Ens}}$	$\sigma_{\mathbf{Ens}}$	$CI95_{\mathbf{Ens}}$
$\boldsymbol{X}$	-0.6%	5.0%	10.8%
$\boldsymbol{Y}$	-2.0%	7.5%	17.4%
$\boldsymbol{N}$	0.9%	4.2%	9.3%

The errors for each component appear to be normally distributed. The statistics of the distribution are presented in Table 7, including a 95% confidence interval of the ensemble comparison error, which is understood as an *estimate* for the range of the comparison errors for the Delft Wind-Assist Series. For the sideforce in particular, a -2 % mean offset indicates there is a systematic under-prediction by the simulation. The negative outliers in Figure 14 correspond to Hull 16, with sharp bilges, where pronounced separation of bilge vortices is expected. Simulation for sideforce is consistently under-predicted for this hull.

6.5 VALIDATION FOR APPENDED CASES

Simulation validation for appended cases is successful for select geometries and operating conditions only. The simulation results for the bilge keel case significantly under-predicts the lateral force. The log-law modelling for the boundary layer is not sufficient to capture separation behaviour at the bilge keel. Results for this case are not reported.

Table 8 Validation details for Hull 1 – Rudder.

	All	***X***	***Y***	***N***
Hull 1 – Rudder 0°, $Fn = 0.168$, β= 0°, 6°, 9°				
$\boldsymbol{r/r_{ref}}$	0.50	0.38	0.39	0.56
Hull 1 – Rudder 6°, $Fn = 0.168$, β= 0°, 6°, 9°				
$\boldsymbol{r/r_{ref}}$	0.77	0.42	1.12	0.32
Hull 1 – Rudder, All operating conditions				
$\boldsymbol{r/r_{ref}}$	0.54	0.45	0.66	0.43

Hull 1 – Rudder, No stall				
r/r_{ref}	0.45	0.43	0.36	0.47

Results for r/r_{ref} for Hull 1 – Rudder are presented in Table 8. The validation set for the Rudder was designed to bring the rudder into the stall regime for rudder angle equal to 6° and $\beta = 9°$. As expected, r/r_{ref} for Hull 1 – Rudder 6° indicates that the comparison error for sideforce exceeds the validation uncertainty. The onset of stall can be identified for this case in Figure 16. If the stalled cases (for rudder angle equal to 6° and $\beta = 9°$) are removed, the validation metric for sideforce is reduced to r/r_{ref}=0.36.

Table 9 Validation details for Hull 34 appendages.

	All	***X***	***Y***	***N***
Hull 34 – Skeg, $Fn = 0.168$, β= 0°, 6°, 9°				
r/r_{ref}	0.50	0.58	0.43	0.10
Hull 34 – Skeg+Barkeel, $Fn = 0.168$, β= 0°, 6°, 9°				
r/r_{ref}	0.64	0.59	0.60	0.52
Hull 34 – Skeg, Skeg+Barkeel, All operating conditions				
r/r_{ref}	0.65	0.64	0.75	0.34

Results for r/r_{ref} for Hull 34 – Skeg and Hull 34 – Skeg+Barkeel are presented in Table 9. For these geometries, the validation metric is less than one for all cases and all entries, and the simulation is validated at validation levels similar to the values given in Table 5.

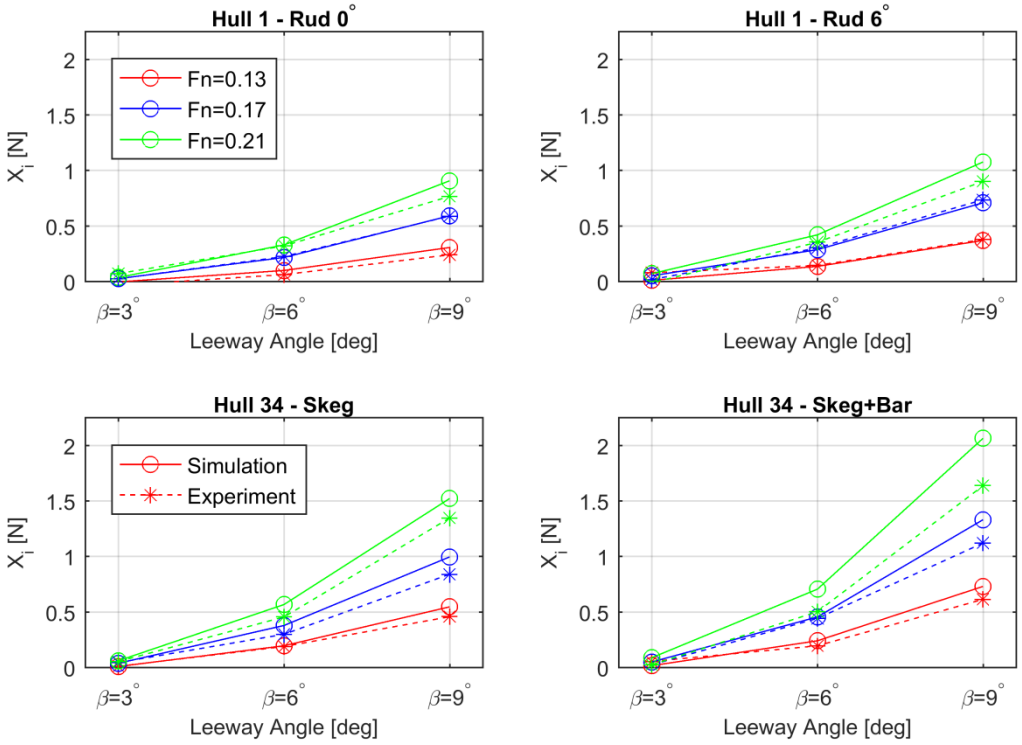


Figure 15 Simulation and experimental results for appended cases for resistance due to leeway.

The results for X_i for appended geometries is subject to the same qualifications outlined above for the bare-hull result. For the appended cases, the resistance increase due to sideforce is generally over-predicted, a trend that also present for the bare hull cases (excepting Hull 16). As with any lifting profile, the production of sideforce for wind-assist vessels is characterised by a wake of vortices. The presence of numerical dissipation may be introducing a non-physical energy loss to the accounting for energy lost in shed vorticity. Though an apparently systematic error is observed, the validation level for this quantity is much too large to consider making a correction.

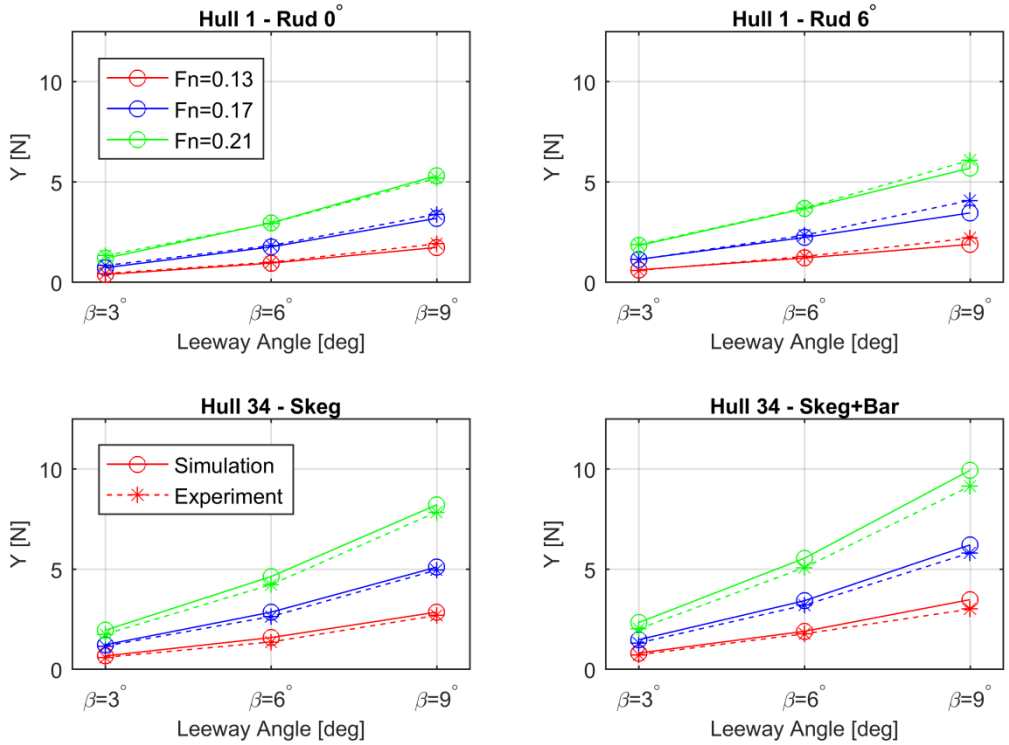


Figure 16 Simulation and experimental results for appended cases for sideforce.

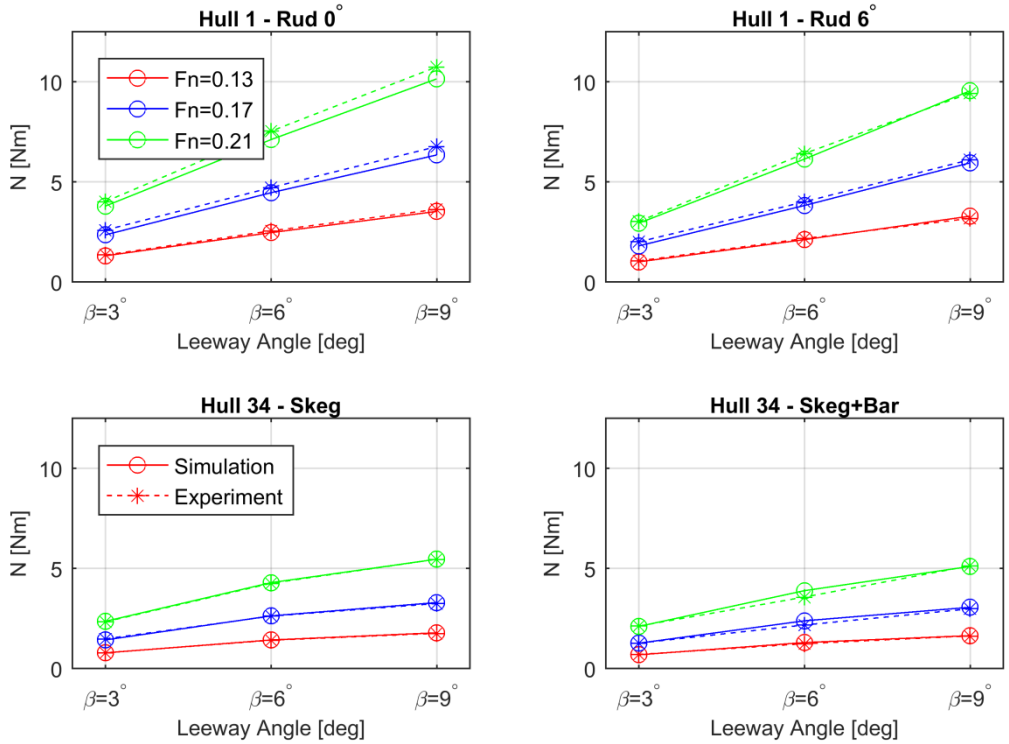


Figure 17 Simulation and experimental results for appended cases for yaw moment.

Simulation and experimental values for sideforce and yaw angle are presented in Figures 16-17. An excellent agreement is observed (when rudder stall angles are removed), indicating that

the simulation methodology may be used to study the sailing balance of wind-assist vessels for these appendage types.

8 CONCLUSION

The validation exercise for RANS-CFD simulation of wind-assist vessels at leeway angles was presented for bare-hull cases and appended cases. The validation methodology was described for point-wise comparison and for multiple validation points. The experimental method was described, with attention placed on the quantification of uncertainty. The uncertainty for numerical simulation was adopted from Part II of this paper. Finally, a series of validation statements was made for the simulation of hulls from the Delft Wind-Assist Series. First, an explicit validation statement was made for the parent hull of the series operating at $Fn = 0.168$ and for leeway angles β= 0°, 6°, 9°. Next, a validation statement was made based on multiple validation points. Here, the knowledge of the numerical uncertainty was limited to three operating conditions for the Hull 1 only. Results for r/r_{ref} were presented for several subsets of the validation set, defined according to the assumptions made for the numerical uncertainty. The validation metric r/r_{ref} was less than one for all cases for the bare-hull validation set, and the simulation method is regarded as validated with validation levels indicated in Table 5. The validation for appended geometries was successful for the Rudder (stalled conditions removed), the Skeg, and Skeg+Barkeel, at validation levels indicated in Table 5.

The effective draft and the center of effort for sideforce are typical derived quantities that will be used to model the performance of wind-assist vessels. The implications of the validation result for resistance, sideforce, and yaw moment on these derived quantities has been outlined. As discussed in Section 6.4, the linear modeling for the T_e, representing the efficiency of the hull, means that data at 9° leeway, for maximum X_i, can be sufficient to determine the effective draft of the vessel. The second quantity of principal interest for this modeling for wind-assist vessels is the center of effort (CoE) for the distribution of hydrodynamic sideforce, related to the course-keeping ability of these vessels. A satisfactory result was obtained for this quantity. For appended hull cases in particular, the CoE was very well predicted. The impact of these appendage types on the course-keeping for wind-assist vessels may be investigated with the RANS-CFD tool.

Simulation for wind-assist vessels is possible with RANS-CFD. Fluid flow around these ships is characterised by the occurrence of separation and by a wake of large vortices, both phenomena that likely challenge modelling assumptions made for the boundary layer and while averaging the Navier-Stokes equations. Modelling separation behaviour and the evolution of vortices in the wake of a wind-assist ship while maintaining a computationally affordable simulation methodology is the principal simulation challenge. In general, the validation level in this exercise was such that modelling errors cannot be distinguished from the uncertainties present in the exercise. One exception is a consistent offset in the comparison error for sideforce for Hull 16 (Figure 12), possibly caused by a failure of the logarithmic wall modeling to capture separation behavior for the sharp bilges of this hull, A correction for this systematic under-prediction may be appropriate. For context, the comparison error is on average 33% larger than the validation level for this hull. The log-law modelling for the boundary layer is also not sufficient to capture

separation behaviour at the bilge keel. The shortcoming of the log-law boundary layer modelling was expected, but the added computational cost of wall-resolved boundary layer modelling was deemed prohibitive in light of the volume of simulations anticipated.

ACKNOWLEDGEMENTS

This research is conducted with the support of the European Commission as part of the Joules Project. The author would also like to thank the Vaderland Fonds for their support. Computations were performed at the SARA supercomputer facility with the sponsorship of NWO Exacte Natuuren Wetenschappen, ENW (NWO Physical Sciences Division), and Numeca International.

REFERENCES

ASME, 2009. *Standard for Verification and Validation in Computational Fluid Dynamics and Heat Transfer,* s.l.: ASME.

Deng, G. B., Guilmineau, E., Queutey, P. & Visonneau, M., 2005. *Ship Flow Simulations with the ISIS CFD Code.* Tokyo, CFD Workship Tokyo.

Deng, G. B., Queutey, P. & Visonneau, M., 2006. *A Code Verificaion Exercise for the Unstructured Finite Volume CFD Solver ISIS-CFD.* Delft, s.n.

Duvigneau, R. & Visonneau, M., 2003. On the role played by turbulence closures in hull shape optimization at model and full scale. *Journal of Marine Science and Technology,* Volume 8, pp. 11-25.

Eça, L. & Hoekstra, M., 2014. A Proceedure for the Estimation of the Numerical Uncertainty of CFD Calculations Based on Grid Refinement Studies. *Journal of Computational Physics,* Volume 262, pp. 104-130.

Hills, R. G., 2006. Model Validation: Model Parameter and Measurement Uncertainty. *Journal of Heat Transfer,* 128(April), pp. 339-351.

ITTC, 2014. Force and Moment Uncertainty Analysis for Planar Motion Test.

ITTC, 2014. Validation and Verification of RANS Solutions.

Jones, R. T., 1946. Properties of low-aspect ratio pointed wings at speeds below and above the speed of sound. *NACA report # 835.*

Keuning, J. A. & Sonnenberg, U. B., 1998. Approximation of the hydrodynamic forces on a sailing yacht based on the 'Delft Systematic Yacht Hull Series'. *HISWA Symposium on Yacht Design and Yacht Construction,* pp. 99-152.

Numeca Int, n.d. ISIS Theoretical Manual.

Queutey, P. & Visonneau, M., 2007. An interface capturing method for free-surface hydrodynamic flows. *Computers and Fluids,* 36(November), pp. 1481-1510.

Roache, P. J., 1997. Quantification of Uncertainty in Computational Fluid Dynamics. *Ann. Rev. of Fluid Mechanics,* Volume 29, pp. 123-160.

Struijk, G., 2015. Hydrodynamics of Wind Assisted Ship Propulsion. *MSc Thesis.*

Surf SARA, n.d. *Description of the Cartesius system.* [Online]
Available at: https://userinfo.surfsara.nl/systems/cartesius/description

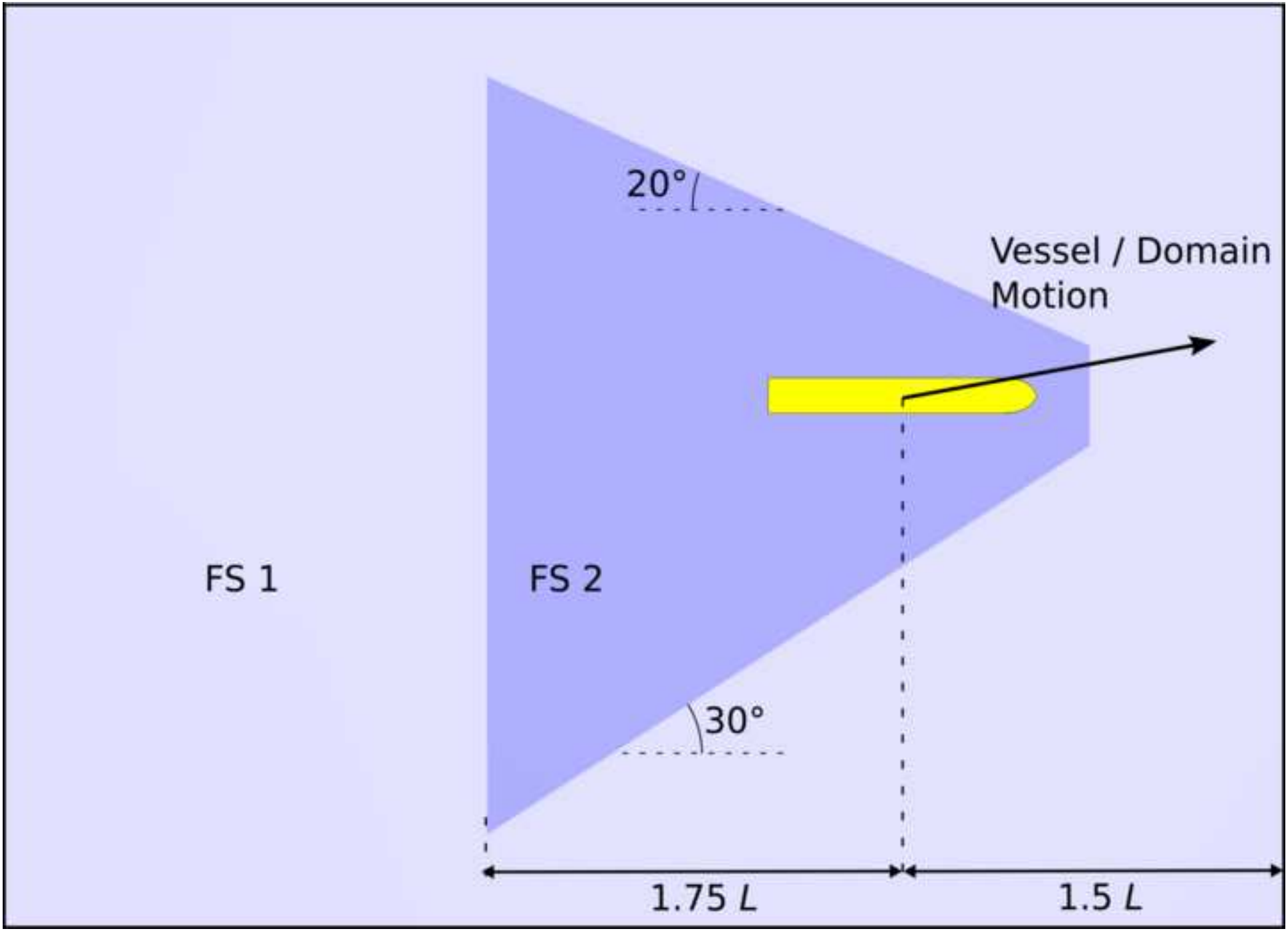
Toxopeus, S. L., 2011. Practical application of viscous-flow calculations for the simulation of manoeuvering ships. *PhD Thesis.*

van der Kolk, N. J., 2016. *Hydrodynamics of Wind-Assisted Ship Propulsion: Modelling of Hydrodynamic Sideforce.* Amsterdam, s.n.

van der Kolk, N. J., Keuning, J. A. & Huijsmans, R. H. M., 2016. *Hydrodynamics of Wind-Assisted Ship Propulsion: Verification of RANS Simulations.* Egmond aan Zee, s.n.

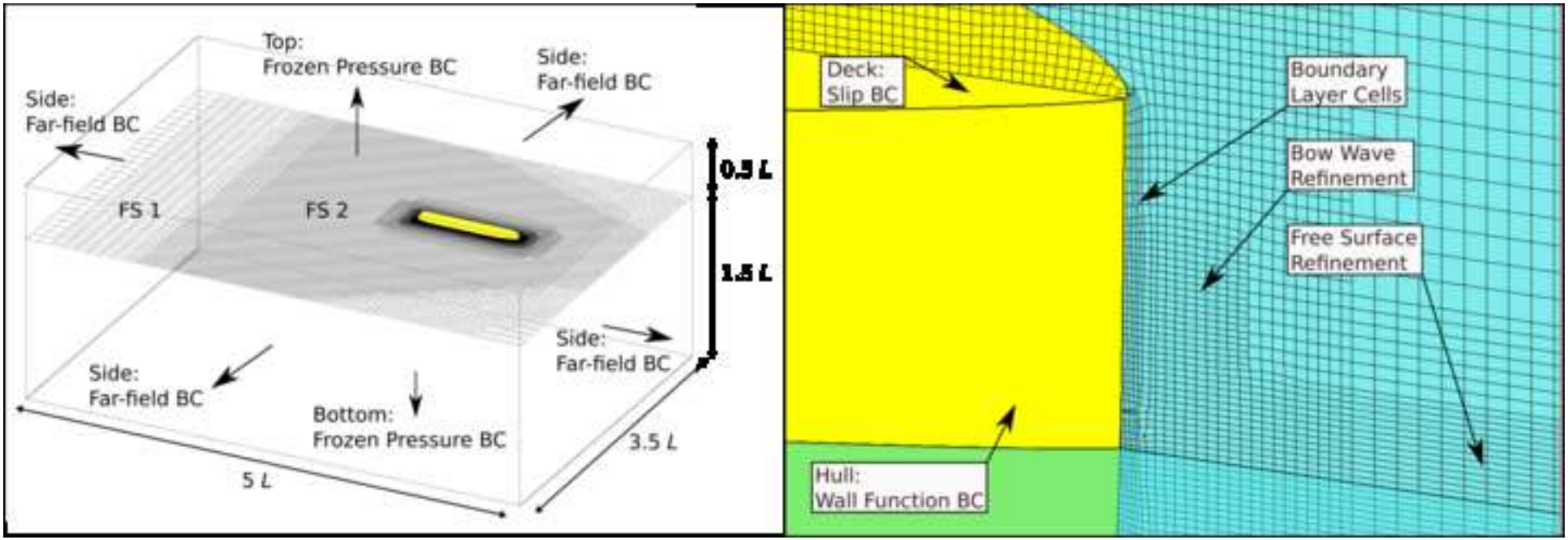
Figure

Click here to download high resolution image



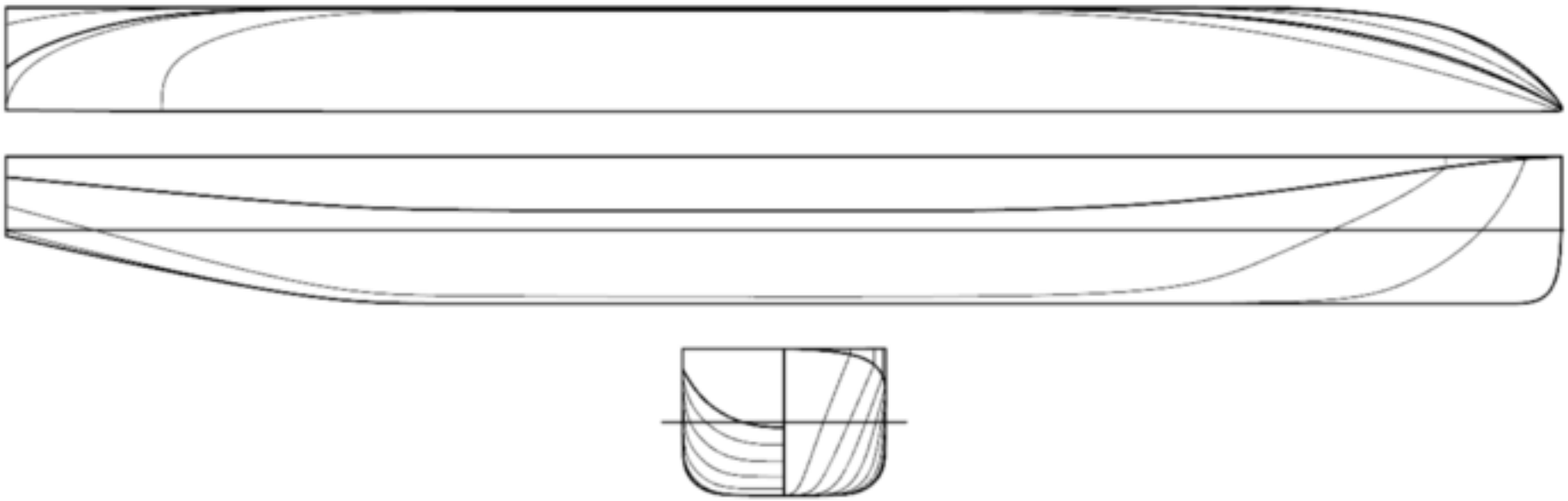
Figure

Click here to download high resolution image



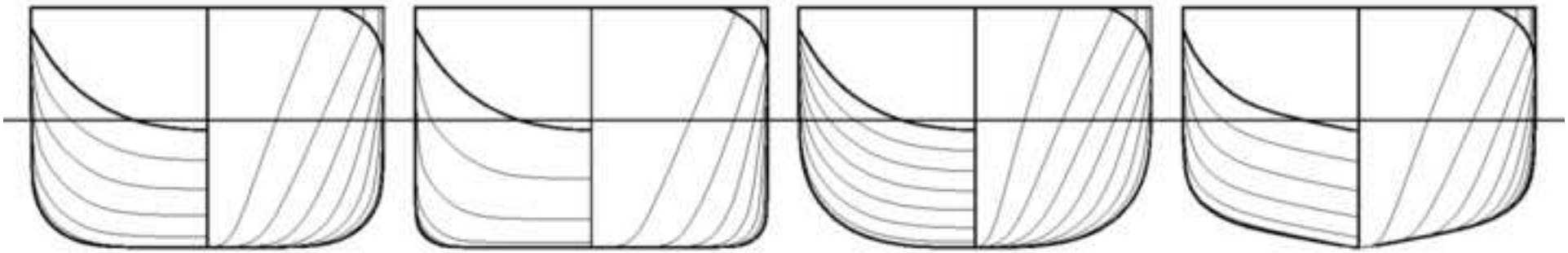
Figure

Click here to download high resolution image



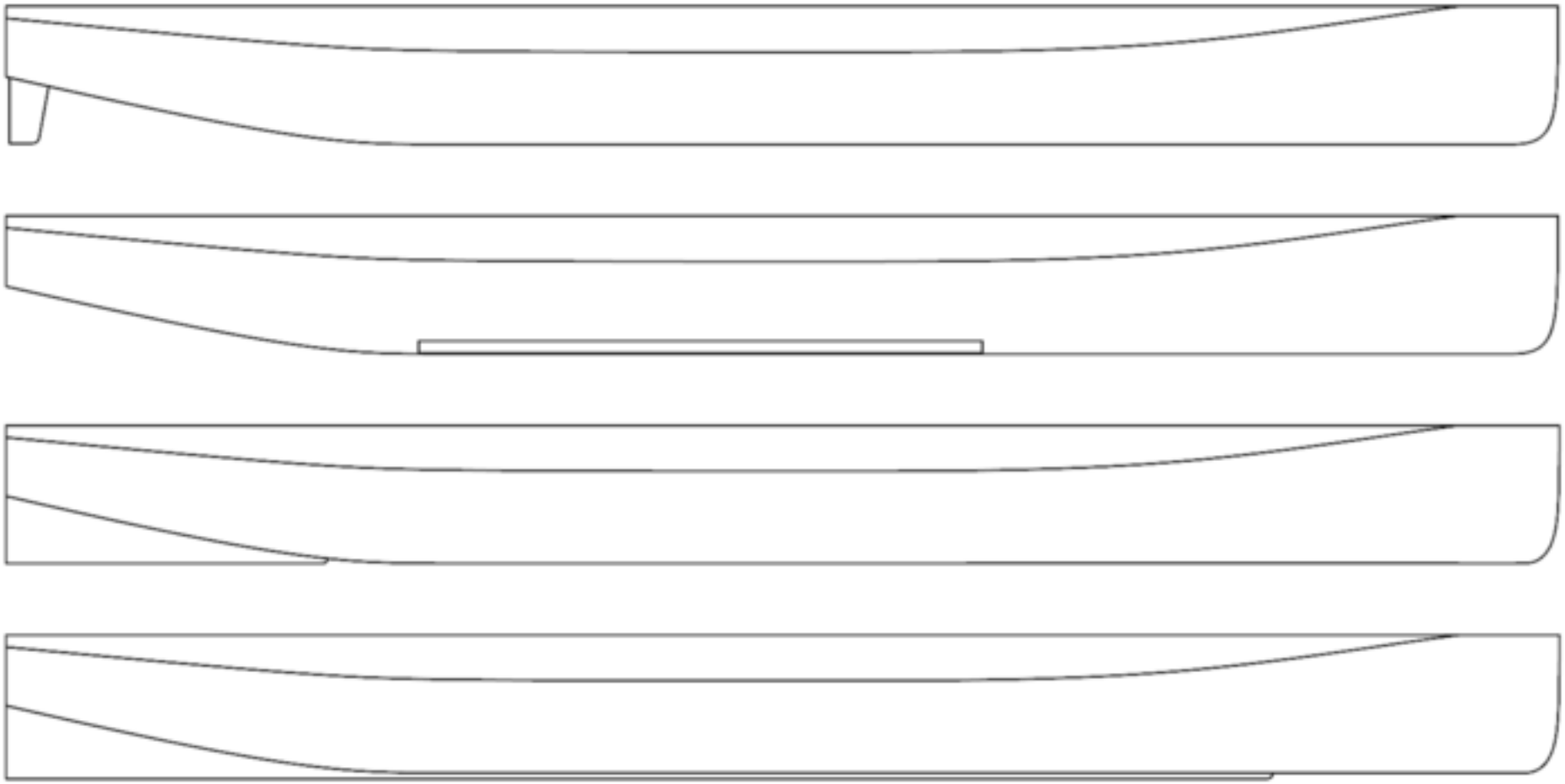
Figure

Click here to download high resolution image



Figure

Click here to download high resolution image



Figure

Click here to download high resolution image

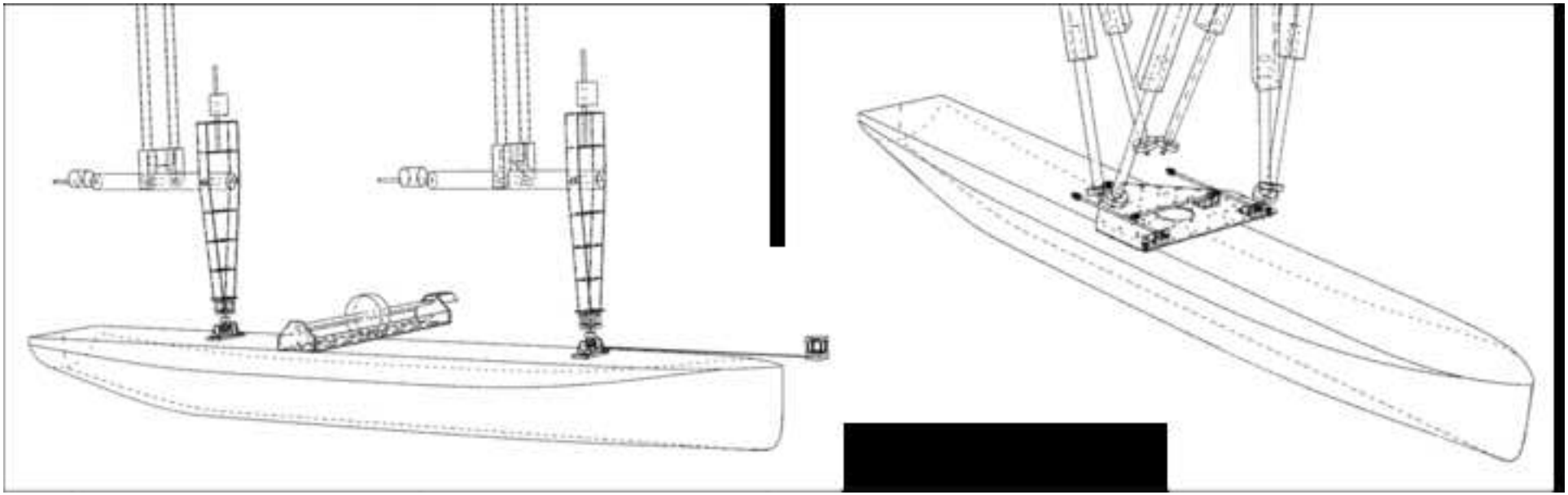
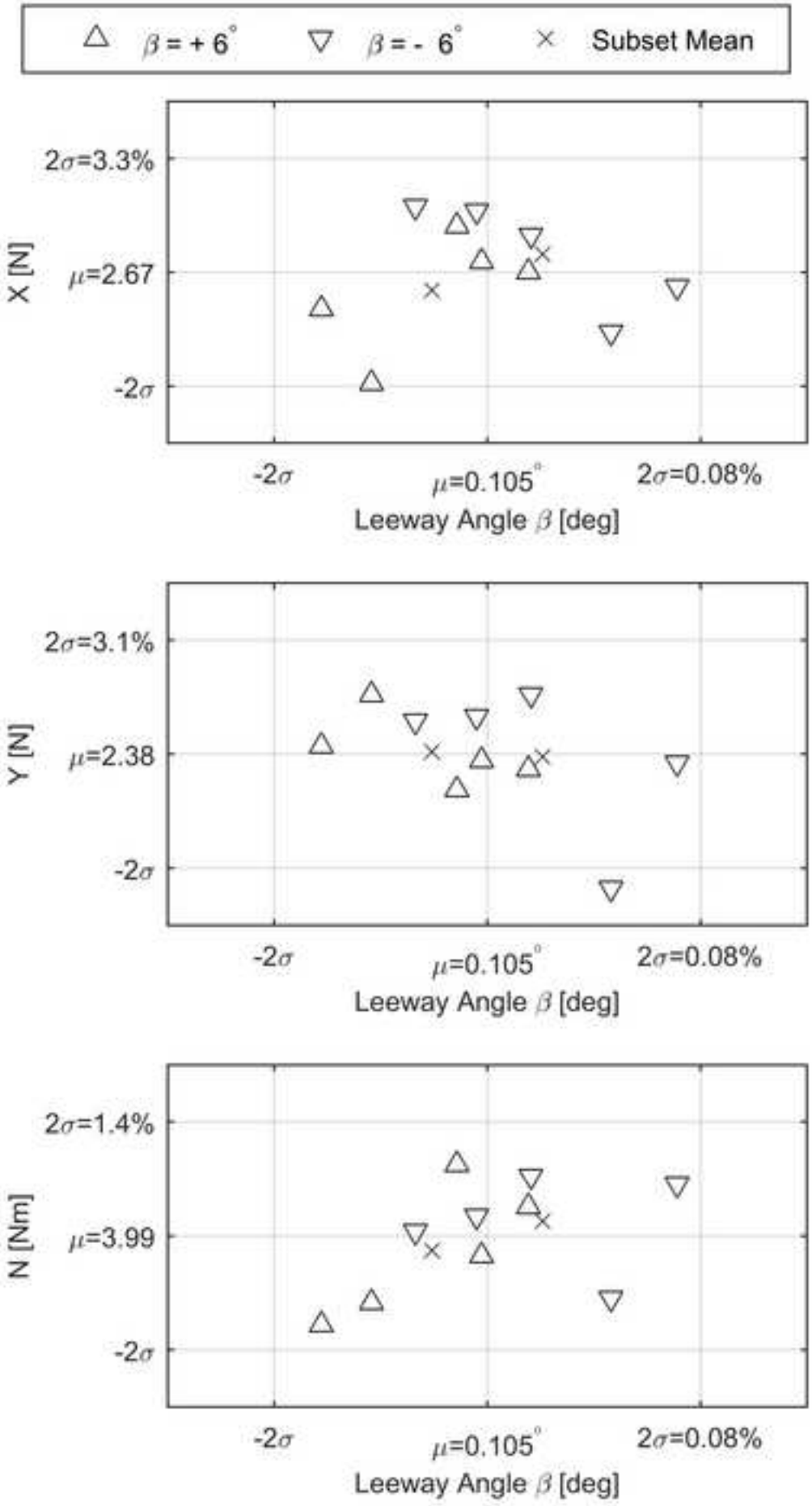
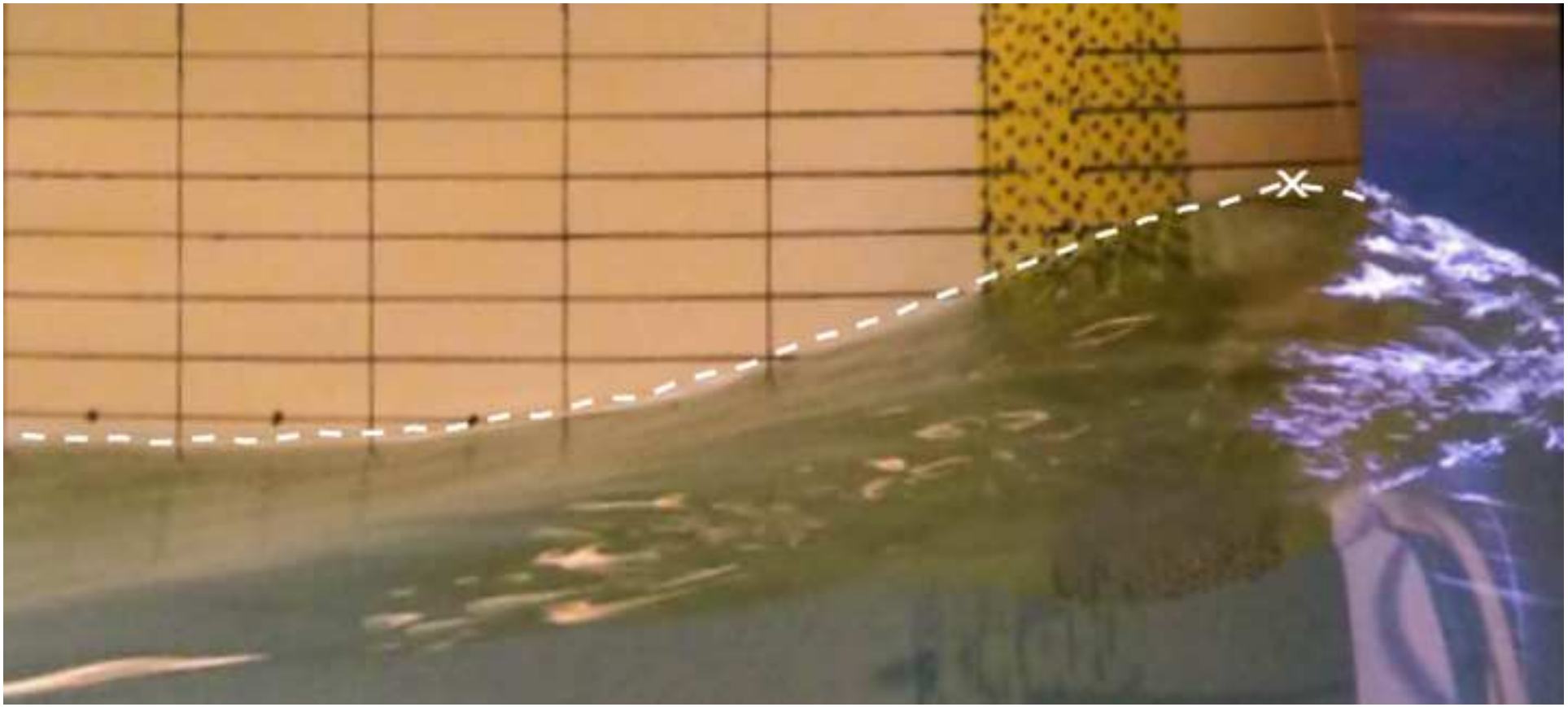


Figure
Click here to download high resolution image



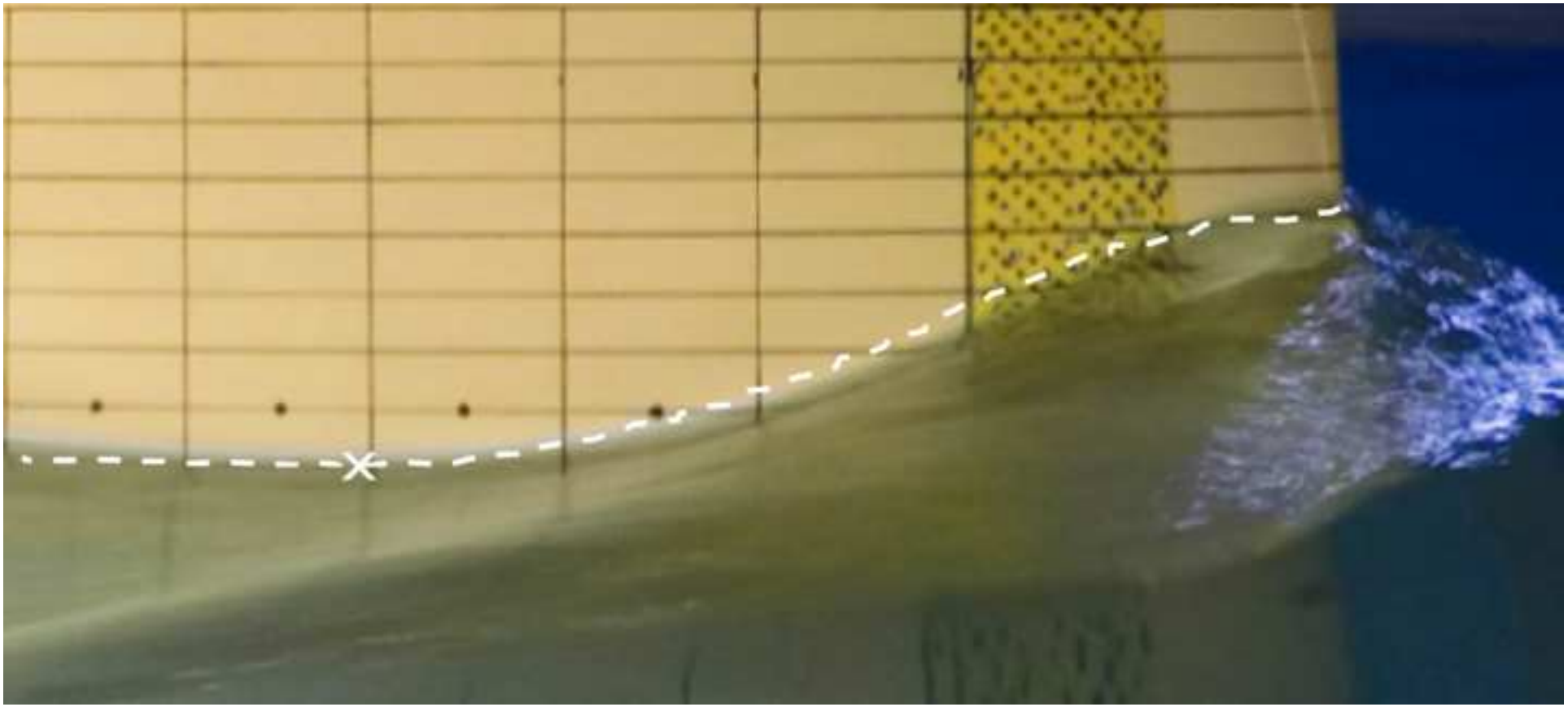
Figure

Click here to download high resolution image



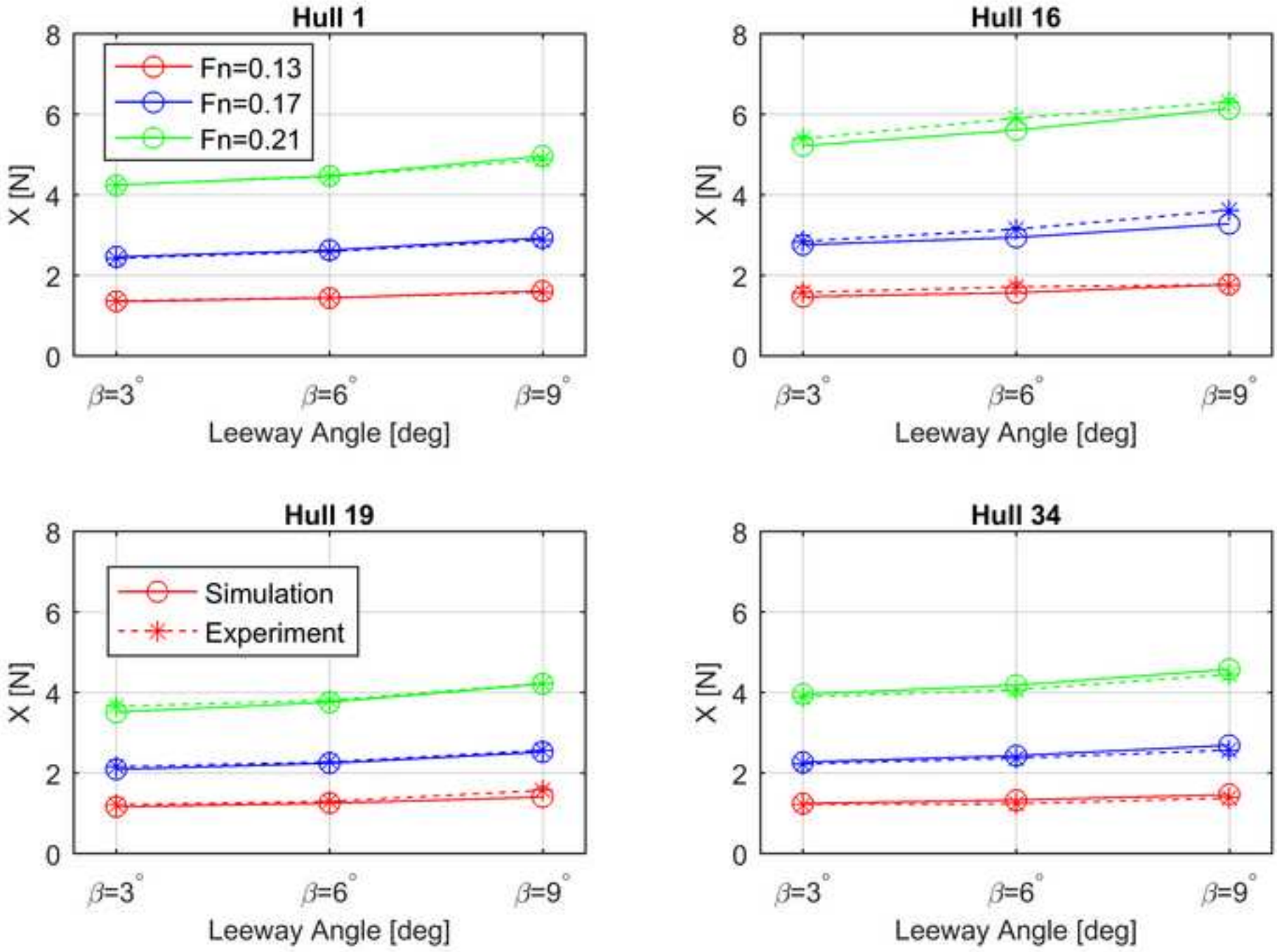
Figure

Click here to download high resolution image



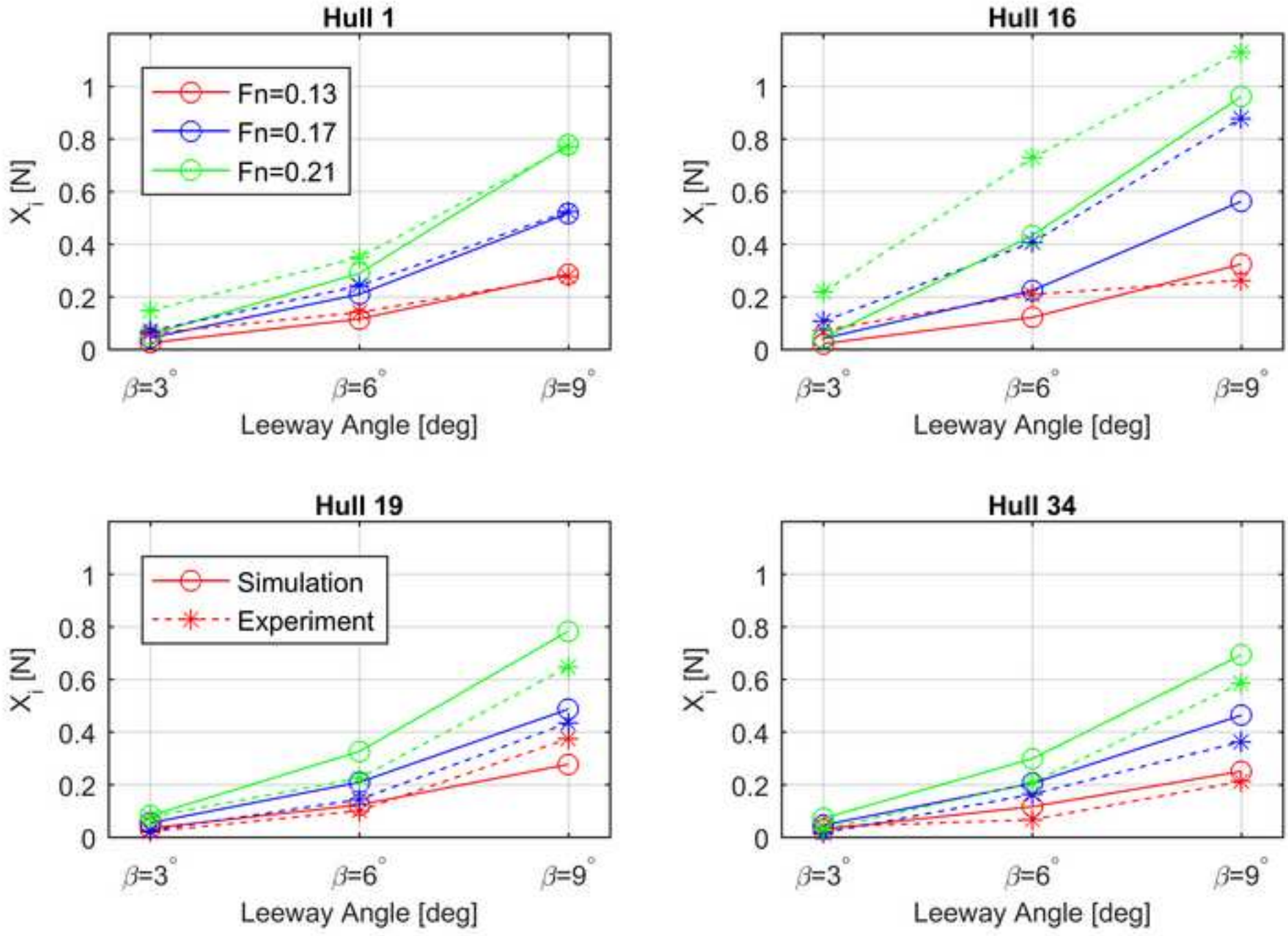
Figure

Click here to download high resolution image



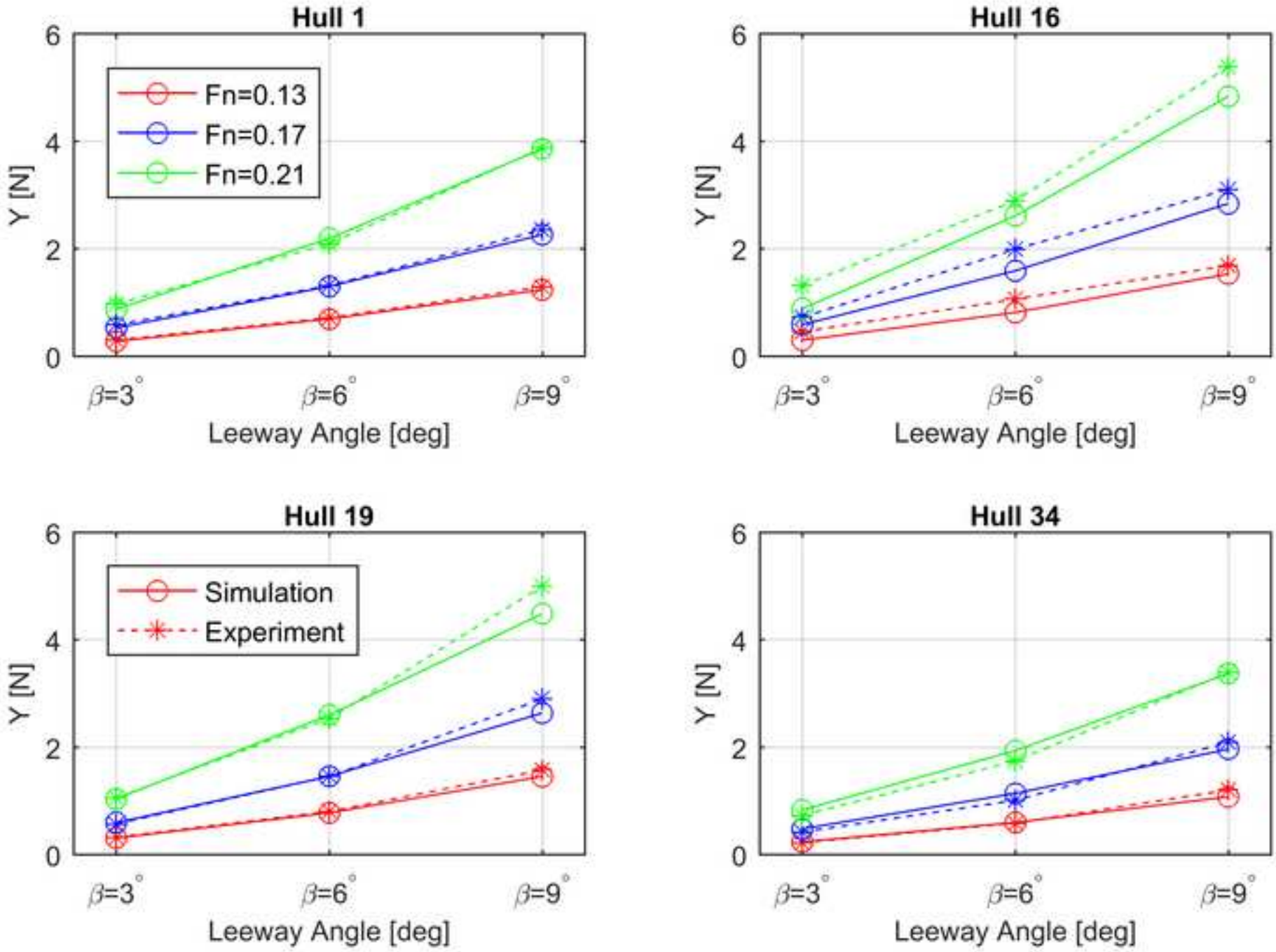
Figure

Click here to download high resolution image



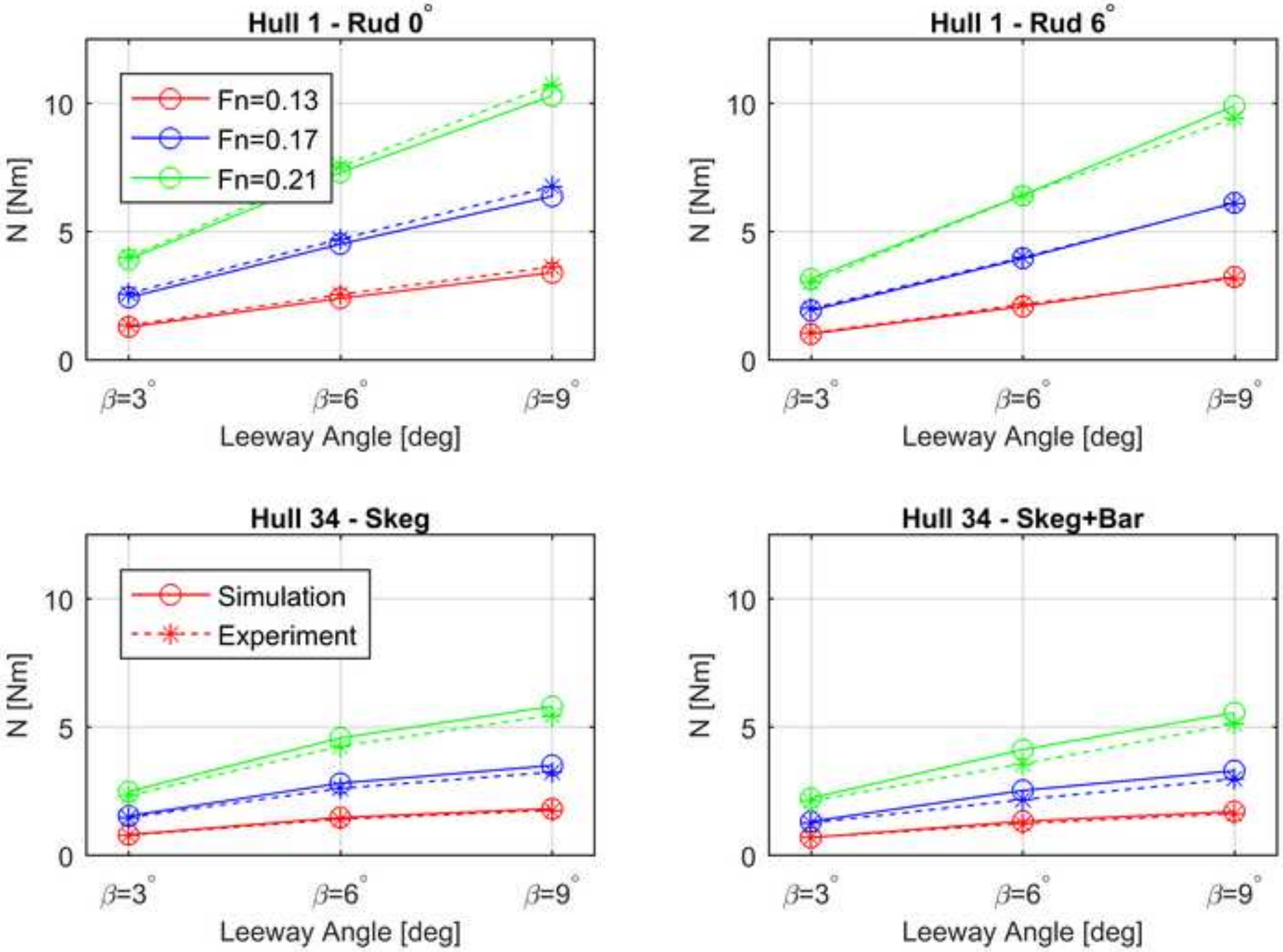
Figure

Click here to download high resolution image



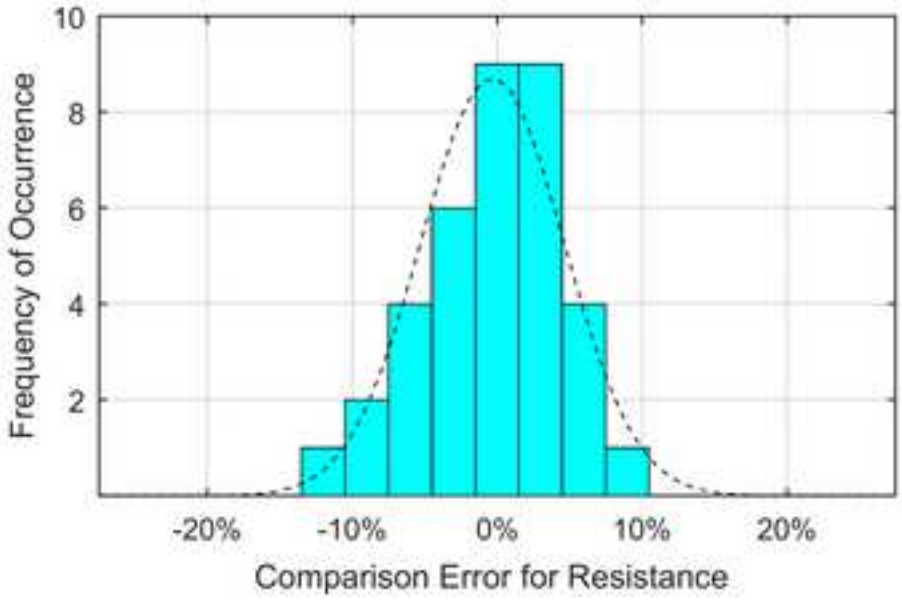
Figure

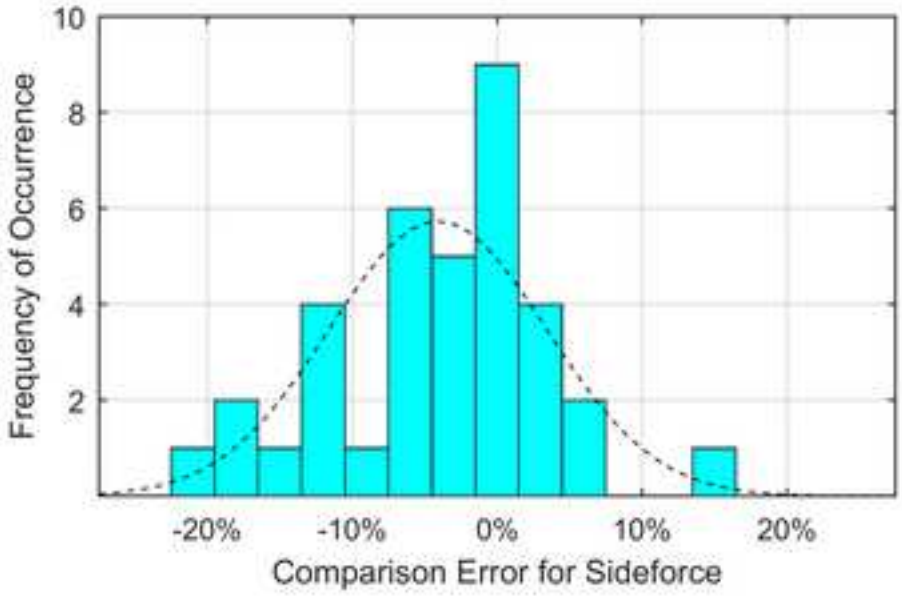
Click here to download high resolution image

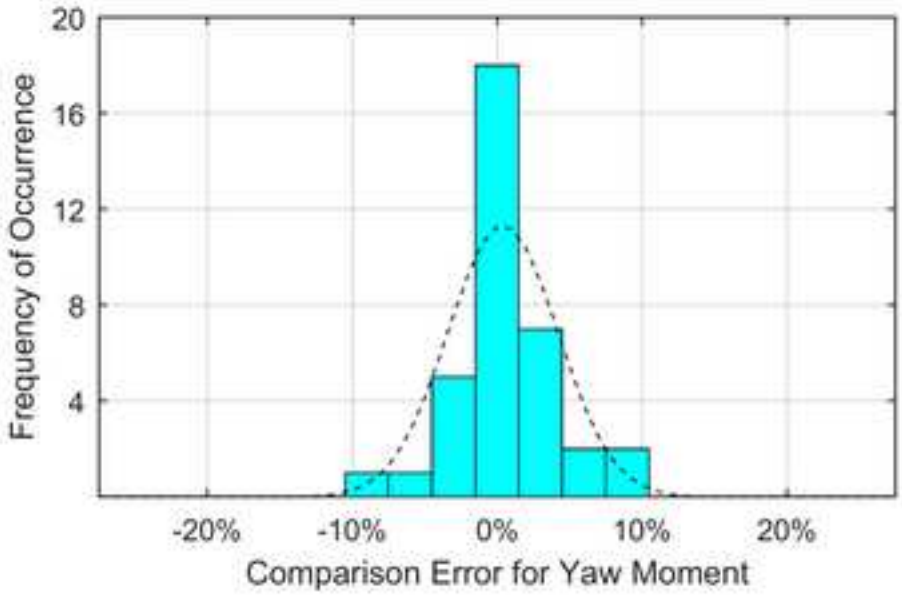


Figure

Click here to download high resolution image







Figure

Click here to download high resolution image

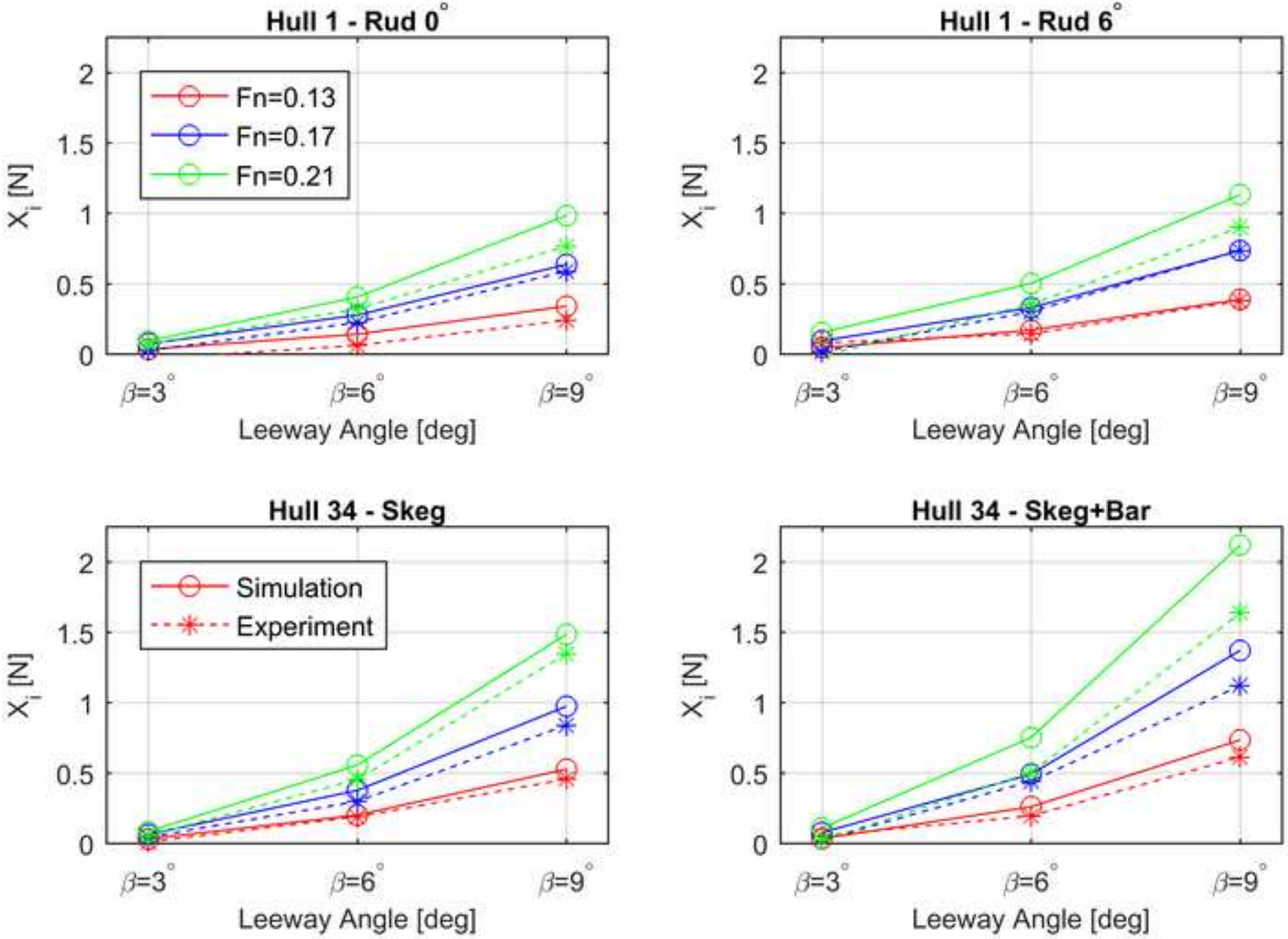
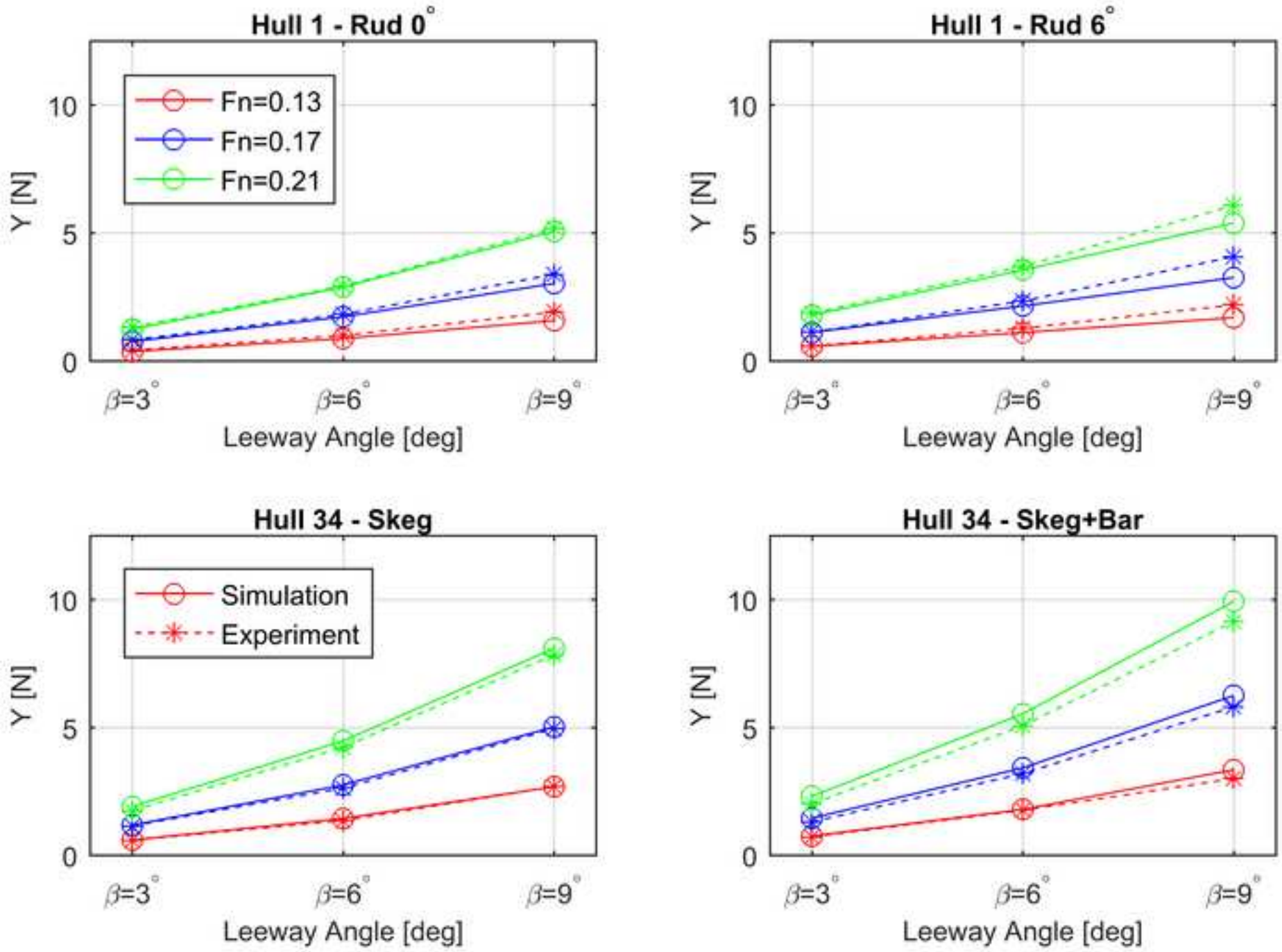


Figure
Click here to download high resolution image



Figure

Click here to download high resolution image

